Mass-independent fractionation of oxygen isotopes during thermal decomposition of divalent metal carbonates: crystallographic influence, potential mechanism and cosmochemical significance

Martin F. Miller [a,*], Mark H. Thiemens [b], Jonathan R. Woodward [c], Edward Bailey [d,1], Paul. F. McMillan [d], Monica M. Grady [a], Caroline Kirk [e,f]

[a] Planetary and Space Sciences, School of Physical Sciences, The Open University, Walton Hall, Milton Keynes MK7 6AA, UK

[b] Department of Chemistry and Biochemistry, University of California San Diego, 9500 Gilman Drive, La Jolla, CA 92093-0356, USA

[c] Graduate School of Arts and Sciences, The University of Tokyo, 3-8-1 Komaba, Meguro-ku, Tokyo, 153-8902, Japan

[d] Department of Chemistry, University College London, Gower Street, London WC1E 6BT, UK

[e] School of Chemistry, University of Edinburgh, Joseph Black Building, David Brewster Road, Edinburgh EH9 3FJ, UK

[f] Earth Sciences, The Natural History Museum, Cromwell Road, London SW7 5BD, UK

[1] *Present address:* Department of Chemical Engineering, Imperial College London, Imperial College Road, Kensington, London SW7 2AZ, UK

[*] Corresponding author.
E-mail address: m.f.miller@open.ac.uk (M.F. Miller)

Abstract

Few physical or chemical processes defy well-established laws of mass-dependent isotopic fractionation. A surprising example, discovered two decades ago, is that thermal decomposition of calcium and magnesium carbonate minerals (conducted *in vacuo*, to minimise back-reaction and isotopic exchange) causes the oxygen triple-isotope compositions of the resulting solid oxide and CO_2 to fit on parallel mass-dependent fractionation lines in $\ln(1 + \delta^{17}O)$ versus $\ln(1 + \delta^{18}O)$ space, with anomalous depletion of ^{17}O in the solid and equivalent enrichment of ^{17}O in the CO_2. By investigating the thermal decomposition of other natural divalent metal carbonates and one synthetic example, under similar conditions, we find that the unusual isotope effect occurs in all cases and that the magnitude of the anomaly ($\Delta'^{17}O$) seems to depend on the room temperature crystallographic structure of the carbonate. A lower cation coordination number (as associated with smaller cation radius) correlates with a $\Delta'^{17}O$ value closer to zero. Local symmetry considerations may therefore be influential. Relative to a reference fractionation line of slope 0.524 and passing through VSMOW, solid oxides produced by thermal decomposition of orthorhombic carbonates were characterised by $\Delta'^{17}O = -0.367 \pm 0.004$ ‰ (standard error). The comparable figure from rhombohedral examples was -0.317 ± 0.010 ‰, whereas from the sole monoclinic (synthesised) specimen it was -0.219 ± 0.011 ‰. The numerical values are, to some extent, dependent on details of the experimental procedure. We discuss potential origins of the isotopic anomaly and propose an ion-radical pair mechanism involving hyperfine coupling between ^{17}O nuclei and unpaired electrons (the 'magnetic isotope effect'). The associated transition state is compatible with that suggested by recent quantum chemical and kinetic studies of the thermal decompositions of calcite and magnesite. An earlier suggestion based on the magnetic isotope effect is shown to be incompatible with the generation of a ^{17}O anomaly, regardless of the identity of the carbonate. We cannot exclude the possibility that Fermi resonance may additionally affect the magnitude of $\Delta'^{17}O$ in some cases. Our findings have cosmochemical implications, with thermal processing of carbonates providing a potential mechanism for the mass-independent fractionation of oxygen isotopes in protoplanetary systems.

Key words:

Oxygen triple isotopes; Mass independent fractionation; Carbonates; Thermal decomposition; Magnetic isotope effect; Cosmochemistry

1. INTRODUCTION

With few – though important – exceptions, chemical or physical process that modify oxygen stable isotope distributions in nature, whether under equilibrium conditions or by kinetic mechanisms, cause the $^{17}O/^{16}O$ ratio to change by approximately half the corresponding change in $^{18}O/^{16}O$. This is related to the mass difference between ^{17}O and ^{16}O (1.0042 Da) being approximately half that between ^{18}O and ^{16}O (2.0042 Da). Isotope ratio modifications that follow this pattern of proportionality are usually referred to as 'mass-dependent' fractionations and are described by well-established laws (Urey, 1947; Bigeleisen and Goeppert-Mayer, 1947; Bigeleisen and Wolfsberg, 1957; Young et al., 2002; Dauphas and Schauble, 2016). In contrast, Thiemens and Heidenreich (1983) reported that ozone generated by electrical discharge in molecular oxygen deviates from this relationship, with the $^{17}O/^{16}O$ and $^{18}O/^{16}O$ ratios changing by an equal amount. Since this discovery of a chemically produced 'mass independent' (or 'non-mass-dependent') isotope effect, several other examples have been documented, usually involving gas phase photochemistry. These include the reaction of CO with the ·OH radical in Earth's atmosphere (Röckmann et al., 1998); photodissociation of CO_2 (Bhattacharya et al., 2000) and of CO (Chakraborty et al., 2012). The occurrence of mass independent isotope effects in nature provides useful tracers and insights to the present and past atmosphere, climate and even the origin of life (Thiemens and Lin, 2019).

Surprisingly, thermal decomposition of calcium and magnesium carbonates is also associated with mass-independent fractionation of the oxygen isotopes (Miller et al., 2002), if the decomposition is conducted under vacuum, to minimise the potential for back-reaction and isotopic exchange between the resulting solid oxide and CO_2. Anomalous depletion of ^{17}O in the solid oxide is accompanied by a corresponding enrichment of ^{17}O in the CO_2. No generally accepted explanation for this finding has since been proposed. Here, we report an investigation of whether the unusual fractionation pattern

occurs during thermal decomposition of other anhydrous divalent metal carbonates and consider whether the magnitude of the isotopic anomaly relates to specific characteristics of the individual carbonates. Most of the empirical data were obtained shortly after the initial report, but have not been published hitherto. Some years later, we also tested a hypothesis based on a hyperfine coupling mechanism (proposed and subsequently published by Buchachenko, 2013) for explaining the experimental findings. Although that test and its outcome were mentioned at a conference (Miller et al., 2012), no data were reported in the abstract; neither have they been published since. We therefore present the details here, together with the (also hitherto unpublished) oxygen triple-isotope measurements of oxides from thermal decomposition of eight different divalent carbonate minerals, for comparison with the Ca and Mg examples reported by Miller et al. (2002).

On the basis of the Buchachenko (2013) mechanism, details of which are discussed below (Section 5.5), all divalent metal carbonates would be expected to exhibit mass-independent fractionation of the oxygen isotopes during the thermal decomposition process, unless the corresponding cation in the univalent state contains no unpaired electrons. In this case, the intermediate cannot be a radical pair and therefore its reactions are not spin-state selective. Because Cu^{+} has electronic configuration $[Ar]3d^{10}$, a definitive empirical test of the hypothesis was to perform controlled thermal decomposition of $CuCO_3$ *in vacuo* and measure the oxygen triple-isotope compositions of the resulting CuO and CO_2. If the proposed mechanism is correct, no ^{17}O anomaly would be produced.

Unfortunately, $CuCO_3$ does not occur in nature. The first reliable synthesis – from heating the hydroxycarbonate minerals azurite and malachite at 500 ± 10 °C for approximately 21 hours duration in CO_2 atmosphere at 20 ± 1 kb pressure – was reported by Ehrhardt et al. (1973), with the structure being published the following year (Seidel et al., 1974). $CuCO_3$ is a grey, monoclinic crystalline solid (space group $Pa\text{-}C^2_S$, cation coordination number 5), reputedly stable in dry air at room temperature for several months. To conduct the experimental test, it was therefore necessary to first prepare a small quantity (~20 mg) of $CuCO_3$, based on the Ehrhardt et al. (1973) procedure.

2. DEFINITIONS AND NOTATION

Measurements of oxygen triple-isotope ratios are, by convention, reported as $\delta^{17}O$ and $\delta^{18}O$ values relative to a specific reference material, usually Vienna Standard Mean Ocean Water (VSMOW). With ^{17}R and ^{18}R as the abundances of the respective minor isotopes relative to the ^{16}O abundance, then by definition:

$$\delta^{17}O = \frac{{}^{17}R_{\text{sample}} - {}^{17}R_{\text{reference}}}{{}^{17}R_{\text{reference}}} \quad \text{and} \quad \delta^{18}O = \frac{{}^{18}R_{\text{sample}} - {}^{18}R_{\text{reference}}}{{}^{18}R_{\text{reference}}} \tag{1}$$

Because the magnitudes of the dimensionless quantities $\delta^{17}O$ and $\delta^{18}O$ are << 1 in natural systems, their values are usually reported as parts per thousand (per mil, ‰). For two chemical entities or phases A and B at equilibrium, the fractionation factors for oxygen isotope exchange, defined by:

$$\alpha^{17/16}_{\text{A-B}} = \frac{{}^{17}R_{\text{A}}}{{}^{17}R_{\text{B}}} = \frac{1+\delta^{17}O_{\text{A}}}{1+\delta^{17}O_{\text{B}}} \quad \text{and} \quad \alpha^{18/16}_{\text{A-B}} = \frac{{}^{18}R_{\text{A}}}{{}^{18}R_{\text{B}}} = \frac{1+\delta^{18}O_{\text{A}}}{1+\delta^{18}O_{\text{B}}} \tag{2}$$

are related by:

$$\alpha^{17/16}_{\text{A-B}} = \left(\alpha^{18/16}_{\text{A-B}}\right)^{\theta} \tag{3}$$

Although few experimental measurements of θ have been reported, calculations (Matsuhisa et al., 1978; Young et al., 2002; Cao and Liu, 2011; Dauphas and Schauble, 2016) for various equilibrium exchange reactions give a range from ~0.522 to a universal high temperature limit value of 0.5305.

Kinetic processes may be described by a comparable formalism (Young et al., 2002; Dauphas and Schauble, 2016). As noted by Young et al. (2002), the masses used to evaluate θ in such cases depend on the isotopic species in motion: reduced masses apply for breaking bonds whereas molecular or atomic masses apply for transport processes. The functional form of θ for kinetic processes involving a triple-isotope system is $\ln(\mu_1/\mu_2)/\ln(\mu_1/\mu_3)$, where μ_i are the reduced, molecular or atomic masses. For the simple case of Graham's Law diffusion, θ varies according to the molecular mass of the diffusing entities, with limiting values of 0.501 and 0.516 (the latter for atomic oxygen in the gas phase). In the transition state theory of chemical kinetics, which describes activation energy-limited kinetic isotope fractionation, the corresponding μ_i terms relate to multiple atoms in complex motion

along the reaction coordinate, modelled as a special vibrational mode with a negative force constant (and thus an 'imaginary' vibrational frequency). In general, as noted by Dauphas and Schauble (2016), for isotopic masses $m_1 < m_2 < m_3$, as in the oxygen triple-isotope system, kinetic fractionation exponents are of smaller magnitude than the canonical high-T equilibrium value, 0.5305.

For a collection of natural carbonate samples (or silicate rocks or minerals, oxides or waters) differing in oxygen isotopic compositions, the distributions of ^{16}O, ^{17}O and ^{18}O similarly conform to a power law relationship:

$$\frac{^{17}R_{\text{sample}}}{^{17}R_{\text{reference}}} = (1+\gamma)\left(\frac{^{18}R_{\text{sample}}}{^{18}R_{\text{reference}}}\right)^{\lambda} \quad (4)$$

where λ and γ are empirical parameters. Whereas θ relates to a specific process, such as isotope exchange under equilibrium conditions, or kinetic fractionation, the exponent is usually designated as λ when the process or cumulative processes are undefined or unknown. In linear format and expressed in terms of $\delta^{17}O$ and $\delta^{18}O$ values, as determined experimentally, Eq. (4) becomes (Meijer and Li, 1998; Miller, 2002):

$$\ln(1+\delta^{17}O) = \lambda \ln(1+\delta^{18}O) + \ln(1+\gamma) \quad (5)$$

In some reports, $\ln(1+\delta^{17}O)$ and $\ln(1+\delta^{18}O)$ are designated as $\delta'^{17}O$ and $\delta'^{18}O$ respectively, following similar terminology introduced by Hulston and Thode (1965) in the context of sulphur multiple isotope ratios. The $\ln(1+\gamma)$ term is a measure of any ordinate offset of the $\ln(1+\delta^{17}O)$ versus $\ln(1+\delta^{18}O)$ linear array from the zero point of the $\delta^{17}O$ and $\delta^{18}O$ scales, usually VSMOW. Defining $\Delta'^{17}O \equiv \ln(1+\Delta^{17}O)$ as the magnitude of any inequality between the two sides of Eq. (5), this parameter represents the $\ln(1+\delta^{17}O)$ offset of an individual sample from a reference mass fractionation line of slope λ and ordinate offset γ. An empirical reference line, such as defined from a collection of samples, may be used; alternatively, the reference line may be of arbitrarily assigned slope (λ_{RL}) and ordinate offset (γ_{RL}). A value of 0.528 is commonly assigned to λ_{RL} (and with $\gamma_{RL} = 0$), corresponding to the VSMOW-SLAP scale for $\Delta'^{17}O$ measurements (Schoenemann et al., 2013).

SLAP is the Standard Light Antarctic Precipitation reference and has $\Delta'^{17}O$ defined to be zero on the VSMOW-SLAP scale. Thus,

$$\Delta'^{17}O = \ln(1 + \delta^{17}O) - \lambda_{RL} \ln(1 + \delta^{18}O) - \ln(1 + \gamma_{RL}) \quad (6)$$

Because the difference between $\ln(1 + \Delta^{17}O)$ and $\Delta^{17}O$ is below the measurement precision limit (~5 ppm) for $\Delta^{17}O < 3$ ‰, which is orders of magnitude greater than nearly all examples in nature, $\Delta^{17}O$ may be conveniently approximated as $\Delta'^{17}O$ without loss of accuracy. This is currently standard practice, for measurements at high precision. Alternatively, $\Delta^{17}O$ may be expressed (exactly) as:

$$\Delta^{17}O = \frac{1 + \delta^{17}O}{\left(1 + \gamma_{RL}\right)\left(1 + \delta^{18}O\right)^{\lambda_{RL}}} - 1 \quad (7)$$

Eq. (6), based on Miller (2002), has been widely adopted, with various assigned values of λ_{RL} (as discussed by Hofmann et al., 2017), with or without the inclusion of a γ_{RL} term. From a practical perspective, it is also useful to include a scaling factor of 10^3 so that the logarithmic terms are then of similar magnitude to the corresponding $\delta^{17}O$ and $\delta^{18}O$ values reported as ‰. Linear regression of the $10^3\ln(1 + \delta^{17}O)$ versus $10^3\ln(1 + \delta^{18}O)$ data from a collection of samples differing in oxygen isotopic composition gives a 'mass fractionation line' of slope λ and ordinate intercept $10^3\ln(1 + \gamma)$ specific to the particular group of samples. There is not necessarily an implied relationship between the individual samples. In practice, the ordinate intercept value $10^3\ln(1 + \gamma)$ may be approximated as $10^3\gamma$ without loss of accuracy. The magnitude of $\Delta'^{17}O$ is not necessarily of physical significance, as a proportion may be attributed to the divergence (or convergence) of the assigned reference line from the linear array formed by the specific group of samples under investigation. Furthermore, a non-zero value of $\Delta'^{17}O$ does not necessarily imply mass-independent fractionation.

The parameter $\Delta^{17}O$ was originally introduced by Clayton and Mayeda (1988) and defined on the basis of approximating the relationship between $\delta^{17}O$ and $\delta^{18}O$ as a linear function; a proportionality constant of 0.52 was usually adopted. For further information on oxygen triple-isotope systematics, see Miller and Pack (2021) and references therein.

3. METHODS

3.1. Samples

Apart from $CuCO_3$, which was synthesised for this investigation, most of the single carbonate mineral specimens used in this study were supplied by the Natural History Museum, London. Sample details are given in Table 1. The use of natural samples ensured that the relationship between the $^{17}O/^{16}O$ and $^{18}O/^{16}O$ ratios would conform to mass-dependent norms, prior to the commencement of thermal decomposition. Rhombohedral (trigonal) carbonates used in the investigation were $CaCO_3$ (calcite), $MnCO_3$ (rhodochrosite), $FeCO_3$ (siderite) and $ZnCO_3$ (smithsonite). These are characterised by cation coordination number 6 and space group *R*3*c*. Additionally, the $MgCO_3$ (magnesite) and $Ca,Mg(CO_3)_2$ (dolomite) samples from Miller et al. (2002) were included. The dolomite structure is characterised by space group *R*3. Orthorhombic carbonates investigated were $CaCO_3$ (aragonite), $SrCO_3$ (strontianite), $BaCO_3$ (witherite) and $PbCO_3$ (cerussite). In such cases the cation coordination number is 9 and the space group is *Pmcn*. Single carbonates with cation radius larger than ~100 pm are generally characterised by the orthorhombic (aragonite) structure. Whereas oxides formed from thermal decomposition of Ca, Sr and Ba carbonates readily recombine with CO_2 on cooling, others (from Mg, Mn, Fe and Zn carbonates) recombine only at high partial pressures of CO_2 (Goldin and Kulikova, 1984). MnO can be handled in air without hydration or exchange.(Sharma and Clayton, 1965).

3.2. Synthesis of $CuCO_3$

$CuCO_3$ was prepared (by EB) at University College London, using high pressure, high temperature reaction between laboratory reagent copper (II) carbonate hydroxide $CuCO_3{\cdot}Cu(OH)_2$ and CO_2 produced *in situ* by thermal decomposition of silver oxalate, $Ag_2(CO_2)_2$. The latter was prepared by adding silver nitrate to oxalic acid solution; the resulting precipitate was washed in absolute ethanol and dried. Approximately 140 mg of silver oxalate was loaded into a platinum capsule which had been sealed at the lower end by spot welding. 80 mg of $CuCO_3{\cdot}Cu(OH)_2$ was then added. A platinum

disc of width slightly greater than the internal diameter of the capsule, and slightly bowed convex side towards the sample, was then placed over the $CuCO_3 \cdot Cu(OH)_2$. Above this, a cylindrical plug of hexagonal boron nitride was tightly fitted. The loaded capsule was then placed in a non-endloaded piston cylinder ('QUICKPress' model, 'Depths of the Earth', Cave Creek, Arizona, USA), and subjected to a pressure of 2 GPa and temperature of 500 °C for 21 hours. X-ray diffraction analysis showed that no azurite, malachite, copper metal or boron nitride were present in the resulting $CuCO_3$. The yield was ~18 mg, which was sufficient for three replicate thermal decomposition experiments.

3.3. Carbonate thermal decomposition procedure and oxygen triple-isotope measurements of the resulting solid oxides

Thermal decompositions of the carbonate mineral specimens, and subsequent determinations of the oxygen triple-isotope composition of the resulting solid oxide phase, were performed at the Open University. For all the rhombohedral and orthorhombic examples, single grains of ~60 μmol (mass ranging from 5.3 mg for magnesite to 16.7 mg for cerussite) were loaded in duplicate into a quartz glass tube (6 mm external diameter) that formed an integral part of a high vacuum system. After outgassing at 100 °C until a vacuum of ~10^{-4} Pa was attained, samples were gradually heated, with constant pumping, until onset of thermal decomposition caused the pressure to rise to ~0.1 Pa, as monitored with a Penning gauge. The temperature was then held constant until CO_2 evolution essentially ceased, after which the temperature was increased in a carefully controlled manner until the pressure again increased to ~0.1 Pa . This incremental heating procedure was repeated over a period of several days. When no further evolution of CO_2 was detected, the temperature was then increased to 900 °C whilst monitoring the pressure, to check that carbonate decomposition was complete[1]. The quartz tube was then flame-sealed, under high vacuum, and the resulting ampoule transferred to a glove box flushed by dry, high-purity nitrogen. Ampoules were opened in this inert atmosphere and individual oxide grains (none of which had fragmented during the heating process)

[1] A slightly higher maximum temperature of ~940 °C was used for the thermal decomposition of witherite.

transferred into a fluorination chamber fitted with a barium fluoride window. The chamber was then sealed, still containing dry nitrogen, removed from the glove box, and coupled to the vacuum system of a facility for infrared laser-assisted fluorination of silicates or oxides. This procedure ensured that the metal oxide grains were not exposed to air. Fluorination of the grains was conducted using excess of BrF_5 vapour, after ensuring that the oxygen 'blank' was negligible. Details of the procedure have been described elsewhere (Miller et al., 1999; Miller et al., 2002). After purification of the ~30 μmol O_2 by cryogenic traps at –196 °C and by adsorption/desorption to/from cryo-cooled 13X zeolite pellets, oxygen triple-isotope ratio analysis was performed using a VG Isotech PRISM III dual inlet mass spectrometer. The original $\delta^{17}O$ and $\delta^{18}O$ data were subsequently recalibrated to VSMOW, based on a recent inter-laboratory investigation (Miller et al., 2020), anchored to direct measurements of VSMOW and SLAP (Pack et al., 2016). It was found that, although the original $\delta^{18}O$ data (and the Open University data reported in the initial study of 2002) were accurately on the VSMOW scale, the corresponding $\delta^{17}O$ values needed adjusting by –0.012 ‰. Because the initial report (Miller et al., 2002) had demonstrated that corresponding enrichment of ^{17}O occurs in the CO_2 produced during thermal decomposition of carbonate examples (calcite and dolomite), accompanying ^{17}O depletion in the solid oxide, we considered it unnecessary to demonstrate a similar finding for the thermal decomposition of the natural carbonate examples used in this investigation, if the solid oxide was shown to be characterised by 'mass-independent' oxygen isotopic composition.

3.3.1. Carbonate thermal decomposition in an applied magnetic field

If a mechanism based on the magnetic isotope effect is responsible for the anomalous isotopic fractionation of oxygen that occurs during the thermal decomposition of divalent metal carbonates, the magnitude of the anomaly ($\Delta'^{17}O$) may – depending on the magnetic flux density – be influenced by the presence of a magnetic field applied during the thermal decomposition process. We therefore heated additional duplicate grains of two of the carbonate examples (siderite and cerussite), sequentially, with the samples located between the poles of an ion pump (fixed) magnet which provided a magnetic field of flux density ~250 mT. Hyperfine couplings are affected by external

magnetic fields within the flux density limits of generally ~1 mT to ~1T , as shown in Fig. 13 of Woodward (2002), although the specific range for individual examples is usually much narrower. Turro et al. (1985) found that an applied magnetic field of 200 mT had no effect on the ^{13}C enrichment in the reactant remaining after partial photolysis of dibenzyl ketone in the solid phase, whereas the corresponding $\alpha^{17/16}$ decreased from 1.10 ± 0.02 to 1.05 ± 0.02 when the magnetic field was applied.

For our test of the influence of an applied magnetic field, it was necessary to use a different extraction line and design of tube furnace from those used in all the other carbonate decomposition experiments. Furthermore, the temperature ramp rate was lower, resulting in a more protracted decomposition period (approximately double that of the other examples). The $\Delta'^{17}O$ values of the resulting metal oxide grains were compared with those obtained by performing the thermal decomposition in an identical manner, using the same experimental facility, but without the applied magnetic field. We note that the wire-wound tube furnaces used to heat all carbonate samples would also have generated a magnetic field, alternating at a frequency of 50 Hz, although with magnetic flux density probably < 3 mT; clearly negligible for the present test. For comparison, the surface flux density of the Earth's magnetic field at the location of the heating experiments is ~ 0.049 mT.

3.3.2. $CuCO_3$ thermal decomposition procedure and oxygen triple-isotope analysis of the decomposition products

For thermal decomposition of $CuCO_3$, a slightly different procedure was adopted than for the other carbonates. In this case, evolved CO_2 was also collected for oxygen triple-isotope measurements. Three single grains, each of ~ 45 μmol (5.5 mg) were heated individually and sequentially in the same extraction line as for other carbonates. Individual grains were loaded and outgassed overnight at room temperature, after which the extraction line was sealed and any pressure rise during a period of 30 minutes recorded using a capacitance manometer. This was found to be 5×10^{-2} Pa; essentially negligible. Gradual heating of the $CuCO_3$ was then commenced, with released CO_2 being trapped in a borosilicate glass finger maintained at –196 °C by liquefied nitrogen. It was observed that thermal

decomposition of the $CuCO_3$ commenced between 250 °C and 300 °C, with maximum gas evolution (corresponding to pressure of 0.8 to 1.2 Pa, uncorrected for blank) occurring at ~390 °C. The pressure subsequently decreased, to a minimum of 0.12 Pa, as the furnace temperature was gradually increased to 550 °C. Further heating, to 600 °C, caused a slight rise in pressure, attributed to the release of O_2 from CuO decomposition. At this stage, the furnace was switched off and allowed to cool slowly, for resorption of O_2. An n-pentane/liquid nitrogen slush bath (–131 °C) was used to purify the CO_2 from any traces of water, after which the gas was transferred cryogenically to a borosilicate glass tube which was then flame-sealed. Similarly, the (quartz) extraction tube containing CuO from decomposition of the carbonate was also flame-sealed, under vacuum, as for the other carbonates in this investigation. The $CuCO_3$ decomposition procedure was completed within one hour. Fluorination of the CO_2 was conducted at the University of California San Diego (UCSD), by reaction for 45 hr with a 1,000-fold excess of BrF_5 in a Ni tube at 800 °C (Bhattacharya and Thiemens, 1989), to give complete conversion to O_2 and CF_4. Isolation and purification of the O_2 for triple-isotope ratio analysis at UCSD was conducted as described previously (Miller et al., 2002).

3.4. Determinations of $\delta^{18}O$, thermal decomposition temperature profiles, phase purity and elemental compositions of the natural carbonates

Whereas the respective $\delta^{18}O$ values of the carbonates were not of particular significance for this investigation, as it was the $\Delta'^{17}O$ values of the solid oxides formed during thermal decomposition that were primarily of interest, measurements of the $\delta^{18}O$ values of the carbonate specimens were made for completeness, using the long-established method of temperature-controlled reaction with concentrated H_3PO_4 (McCrea, 1950) and isotope ratio measurements of the released CO_2, in conjunction with appropriate fractionation factors.

To compare the relative thermal decomposition profiles of the carbonate minerals as a function of temperature, thermogravimetric analysis (TGA) was conducted (by MMG), using a Netzsch TGA system (model STA 449 C) in conjunction with evolved gas analysis (EGA) using a Hiden HPR20 quadrupole mass spectrometer. Fine-grained samples were loaded into a Pt bucket (with lid) and

heated in a flow of helium (53.8 mL min^{-1}), at a ramp rate of 0.5 °C min^{-1} to 1000 °C, except for witherite, which was heated to 1200 °C. In all cases, the thermal decompositions profiles would not be expected to be identical to those during the protracted thermal decompositions conducted for isotope ratio measurements of the decomposition products, because of the much slower and variable temperature ramp rates during the latter process. In a kinetic study of the thermal decomposition of calcite, Wang et al. (2017) showed that the decomposition profile was shifted to higher temperatures when the calcite was heated in a flow of nitrogen (30m L min^{-1}) rather than in vacuum (10^{-3} Pa); the same authors found that a similar shift – though of much smaller magnitude – also occurred when the ramp rate was increased from 7.5 to 10 °C min^{-1}. A comparative assessment under controlled and constant conditions does, however, provide useful information on the relative stabilities of the carbonates investigated in this study.

For determining the phase purity of the carbonate mineral specimens, X-ray powder diffraction analysis was performed (by CK) at the Natural History Museum, London, using a Nonius diffractometer with Cu K_α radiation and an INEL CPS120 detector. Elemental compositions of the carbonate minerals were determined by electron probe microanalysis at the Open University, using a Cameca SX100 instrument.

4. RESULTS

4.1. Oxygen triple-isotope measurements

4.1.1. Oxides formed from the rhombohedral and orthorhombic carbonates

A compilation of the oxygen triple-isotope data from this investigation is provided in Table 2. From the respective mean values of replicate measurements of the ten solid oxides produced by thermal decomposition of the natural anhydrous carbonates, a linear array of slope 0.5243 ± 0.0011 (standard error) can be derived in $10^3\ln(1 + \delta^{17}O)$ versus $10^3\ln(1 + \delta^{18}O)$ space, with ordinate intercept of –0.343 ± 0.023 relative to VSMOW, as shown in Fig. 1. The slope of the array is in accord with mass-dependent fractionation, but the magnitude of its displacement from VSMOW

identifies isotopically anomalous behaviour during the thermal decomposition process. It is evident that all the natural carbonates investigated here exhibit such behaviour. Lower scatter of individual data points about $10^3\ln(1 + \delta^{17}O)$ versus $10^3\ln(1 + \delta^{18}O)$ regression lines – leading to lower standard error values associated with the respective slope and intercept – has been reported from measurements on silicates: for example, 0.0004 from replicate measurements (also conducted using the same Open University facility) of eight eclogitic garnets (Rumble et al., 2007) and similarly from measurements of fifteen diverse natural silicates conducted at the University of Okayama (Tanaka and Nakamura, 2013). This indicates that the divalent metal oxide data may be subject to small, second-order effects, although variation between replicates contributes to the observed degree of scatter. In the initial report (Miller et al., 2002), coincidentally, the triple-isotope regression line given by replicate measurements of CaO produced from thermal decomposition of calcite reference materials NBS 18 and NBS 19 was 0.5241 ± 0.0009, with the corresponding value for the evolved CO_2 being 0.5239 ± 0.0009. Those two essentially parallel mass-dependent fractionation arrays were separated by a $10^3\ln(1 + \delta^{17}O)$ value of 0.41. For the present investigation, we therefore assign a reference line slope value λ_{RL} of 0.524 and set γ_{RL} to be zero, for defining $\Delta'^{17}O$ in Eq. (6). This avoids the magnitude of $\Delta'^{17}O$ being dependent (as an artefact) on the associated $\delta^{18}O$ value, in contrast to reporting our $\Delta'^{17}O$ data on the VSMOW-SLAP scale (λ_{RL} = 0.528, γ_{RL} = 0), for example.

With reference to Table 2, duplicate grains of siderite heated together in the presence of an applied magnetic field, strength ~0.25 T, produced FeO characterised by $\Delta'^{17}O$ values of –0.293 and –0.299 ‰, whereas in the absence of an applied magnetic field the corresponding data were –0.286 and –0.297 ‰. All these results are identical, within measurement precision. Measurements of the two other duplicate FeO grains from siderite decomposition reported in Table 2 were conducted earlier, using a different extraction line and less protracted heating period. The observation that significantly more negative $\Delta'^{17}O$ values (–0.394 and –0.405 ‰) were obtained during the initial measurements is probably due to the use of different experimental conditions, illustrating the sensitivity of the magnitude of $\Delta'^{17}O$ to details of the carbonate decomposition procedure. Further evidence is provided

by the consistently smaller magnitude of $\Delta'^{17}O$ when metal oxides were generated by infrared laser heating of carbonate samples (calcite, magnesite, dolomite) during a period of only 1–2 hours, rather than when a much slower and more controlled rate of heating, by tube furnace, was adopted (Miller et al., 2002). Clearly, there are several variables that need to be controlled individually before substantive conclusions can be made.

Although duplicate grains of cerussite were also heated in the presence/absence of an applied ~0.25 T magnetic field, as for the siderite, the conclusive finding that the presence of the applied magnetic field had no effect on the $\Delta'^{17}O$ value of the FeO produced from siderite, together with poorer $\Delta'^{17}O$ reproducibility of PbO duplicates produced in the presence of the applied magnetic field (–0.353 and –0.322 ‰ respectively), led to the PbO duplicates produced in the absence of the applied magnetic field not being analysed for oxygen triple-isotope composition.

From the data compilation in Table 2, metal oxides derived from thermal decomposition of the six different calcite isotype minerals (rhombohedral structure) were characterised by a mean $\Delta'^{17}O$ value of –0.317 ± 0.010 ‰ (standard error). This compares with –0.367 ± 0.004 ‰ for the metal oxides formed from the four aragonite isotypes (orthorhombic carbonates). If the final batch of replicate results for siderite and cerussite (identified with an asterisk in Table 2) are excluded, because of the slightly different experimental conditions of thermal decomposition, then the respective mean values become –0.329 ± 0.017 and –0.374 ± 0.008 ‰. Also, the regression line shown in Fig. 1 then becomes slightly steeper: $10^3\ln(1 + \delta^{17}O) = (0.5248 \pm 0.0013)\,10^3\ln(1 + \delta^{18}O) – (0.363 \pm 0.028)$.

4.1.2. CuO and CO_2 formed from thermal decomposition of the synthesised $CuCO_3$

The relationship between the oxygen triple-isotope compositions of the CuO and CO_2 formed from the three replicate thermal decompositions of individual grains of $CuCO_3$ is illustrated in Fig. 2. From mass balance considerations, the $\delta^{17}O$ and $\delta^{18}O$ values of the $CuCO_3$ may be inferred, from which the corresponding $\Delta'^{17}O$ value relative to the assigned reference line is seen to be indistinguishable from zero. For comparison, recent measurements at the Open University of two widely-used silicate standards for oxygen isotope measurements, San Carlos olivine and University of Wisconsin garnet

(UWG-2) respectively, gave $\Delta'^{17}O$ values of –0.020 ± 0.003 and –0.023 ± 0.001 ‰, when recalculated from the corresponding values on the VSMOW-SLAP scale as reported by Miller et al. (2020). The $CuCO_3$ synthesised for this investigation clearly conforms to mass-dependent distribution of the three oxygen isotopes. A $\delta^{18}O$ shift of –2.4 ‰ was associated with complete thermal decomposition of the $CuCO_3$ to CuO, together with the $\delta^{18}O$ value of the evolved CO_2 being 1.2 ‰ greater than in the $CuCO_3$. The corresponding fractionation line slope in $10^3\ln(1 + \delta^{17}O)$ versus $10^3\ln(1 + \delta^{18}O)$ space is ~0.61 (0.602 from decomposition experiment #2 data; 0.623 from decomposition experiment #3), which clearly exceeds the maximum theoretical value of 0.5305 associated with mass-dependent fractionation (Matsuhisa et al., 1978; Young et al., 2002; Dauphas and Schauble, 2016). Although the $\Delta'^{17}O$ value of the resulting CuO (–0.219 ± 0.011 ‰) is more positive than as obtained from the other divalent metal oxides, it nevertheless demonstrates that the mechanism suggested by Buchachenko (2013) cannot be the correct explanation for the ^{17}O depletion in the metal oxides (and associated ^{17}O enrichment in CO_2) formed during thermal decomposition of divalent metal carbonates. This was acknowledged in that same paper, with the isotope effect being described as 'extremely enigmatic.' In subsequent papers (Buchachenko and Lawler, 2017; Buchachenko, 2018) however, the same mechanism was offered as an explanation for the unusual oxygen triple-isotope fractionation during carbonate thermal decomposition, but without reference to the result of $CuCO_3$ decomposition. We infer that, in those later papers, the Buchachenko (2013) mechanism was still considered to be a valid explanation of the thermal decomposition findings reported by Miller et al. (2002) for calcium and magnesium carbonates. The implication is that thermal decomposition of $CuCO_3$ proceeds via a modification of the published hypothesis. In Section 5.5, we re-evaluate the Buchachenko (2013) mechanism in detail.

We cannot exclude the possibility that, compared to the heating of other divalent metal carbonates, the much shorter duration of the $CuCO_3$ thermal decomposition procedure, as necessitated by the need to collect the released CO_2, contributed to the $\Delta'^{17}O$ value of the resulting CuO being slightly closer to zero than would otherwise have been the case. During the peak release of CO_2 from $CuCO_3$ (at

~390°C), the gas pressure in the extraction line was, for a brief period, an order of magnitude greater than during the more protracted thermal decompositions of the natural mineral samples. The higher pressure might have resulted in greater oxygen isotopic exchange between the released CO_2 and the residual solid phase at elevated temperatures; we were not able to quantify to what extent (if any) such exchange actually occurred.

4.2. $\delta^{18}O$ measurements, thermal stability and purity of the natural carbonates

The $\delta^{18}O$ values of the carbonate minerals, as determined by the McCrea (1950) method during this investigation, are presented in Appendix A, Table A.1. Because several of the specimens (especially siderite) were not phase pure, as discussed below, there is some uncertainty about the accuracy of the data obtained by application of published carbonate-H_3PO_4 equilibration fractionation factors for the individual minerals. We have included these data, nevertheless, as an indication of the respective $\delta^{18}O$ changes associated with carbonate thermolysis. A comparison of the CO_2 thermal release profiles as determined from TGA/EGA measurements is presented in Fig. 3 and illustrates the wide range of thermal stabilities of the natural carbonate mineral specimens. The results of electron probe microanalysis and X-ray powder diffraction measurements are presented in the Supplementary Information (Electronic Annex). Only the aragonite and cerussite specimens were found to be essentially free of other phases. The calcite was of slightly lower purity (>99.5 %); smithsonite and witherite specimens were ~98 % pure. In contrast, ~5 % $CaCO_3$ was detected in the strontianite, whereas the rhodochrosite was found to contain ~9 % $FeCO_3$ together with ~0.7 % $MgCO_3$. The siderite example contained the greatest quantity of a secondary mineral, ~23 % $MgCO_3$ together with ~0.2 % $MnCO_3$. For the present investigation, the presence of minor or trace quantities of impurities was not critical to establishing whether mass-independent fractionation of oxygen isotopes occurred during the thermal decomposition process.

Thermal decomposition of the natural divalent carbonate specimens resulted in a range of $\delta^{18}O$ shifts in the solid phase, including significant differences between replicates. The latter variations are most probably attributable, at least in part, to variations in the respective protracted heating profiles.

Because pairs of grains were subjected to the same thermal profile during the decomposition experiments, it is unsurprising that the $\delta^{18}O$ shifts tend to cluster in pairs. Fig. 4 illustrates this, together with the respective peak temperatures of CO_2 release as determined by TGA/EGA. In the case of cerussite, the most labile of the carbonates investigated (and of high purity), pairs of grains heated in two separate experiments produced similar and negative $\delta^{18}O$ shifts, of –7.6 ± 0.3 ‰ during the transition from carbonate to solid oxide. Rhodochrosite decomposition was also characterised by a negative shift in $\delta^{18}O$ during the formation of MnO, although of smaller magnitude (–2.0 ± 0.2 ‰). In contrast, MgO formation from magnesite was accompanied by positive $\delta^{18}O$ shifts of up to 2 ‰, whereas decomposition of the same specimen reported previously (Miller et al., 2002) was accompanied by negative shifts of similar magnitude. Data also reported in the same study showed that thermal decomposition of the carbonatite (calcite) reference material NBS 18 could – surprisingly – proceed with essentially no change in $\delta^{18}O$; the resulting solid oxide being within 0.1 ‰ of the accepted value of 7.20 ‰ for NBS 18 (Coplen et al., 1983), yet the corresponding $\delta^{17}O$ value was anomalously low, relative to mass-dependent composition. Similarly, CO_2 released from NBS 18 could also be characterised by negligible shift from the $\delta^{18}O$ value of the precursor carbonate, whereas the associated $\delta^{17}O$ value was anomalously high. Larger shifts of $\delta^{18}O$ (~ –2.8 ‰) in both decomposition products from NBS 18 were also noted, from replicates, yet without significant variation of the corresponding $\Delta'^{17}O$ value.

Uniquely among the carbonates investigated here, thermal decomposition of witherite is characterised by a bimodal CO_2 release, as revealed by TGA/EGA. For the temperature ramp rate used (0.5 °C min^{-1}), CO_2 evolution initially occurred from ~820 to 980 °C, with a maximum at ~950 °C. As the temperature was increased further, a second release of CO_2 commenced, resulting in maximum gas evolution at 1047 °C and the completion of decomposition by 1060 °C. For investigation of oxygen triple-isotope changes accompanying the carbonate to solid oxide transition, duplicate grains of witherite heated together to a maximum of ~940 °C resulted in $\delta^{18}O$ shifts of –9.1 and –16.0 ‰ respectively. This is a considerably greater difference between duplicates than occurred

during thermal decomposition of any of the other divalent carbonate specimens. Despite this, however, the $\Delta'^{17}O$ values of the resulting BaO differed by only 0.007 ‰, which is at the experimental precision limit[2]. Although the vacuum line was at baseline pressure after the final (overnight) heating step of ~940 °C, it is probable, on the basis of the TGA/EGA findings, that decomposition of the witherite was incomplete. We therefore include the $BaCO_3$ thermal decomposition results with this proviso, which may affect the accuracy of the $\Delta'^{17}O$ measurements in this particular case, although it is evident nevertheless that thermal decomposition was accompanied by mass-independent fractionation.

5. DISCUSSION

5.1. Relationship between $\Delta'^{17}O$ of the metal oxides and crystallographic structure of the parent carbonate

Despite the variability between replicate $\Delta'^{17}O$ measurements of individual metal oxides, there appears to be an association between the respective mean $\Delta'^{17}O$ values and whether the parent carbonate has a rhombohedral, orthorhombic or monoclinic structure (at room temperature). This is illustrated in Fig. 5, with cation radius data from Shannon (1976). The carbonate structural type, which controls the cation coordination number, is determined by the cation radius. A rhombohedral structure is adopted when the cation radius is ~70 to 100 pm, whereas the orthorhombic form occurs when the cation radius is larger. Calcium carbonate, uniquely, adopts both structural forms, as calcite (rhombohedral) and aragonite (orthorhombic). The cation radius in $CuCO_3$, which is monoclinic, is only 65 pm. It is noteworthy that, if a $\Delta'^{17}O$ value of close to –0.40 ‰ for FeO is most appropriate for comparison with the other metal oxide examples produced using the same experimental facility and procedure (as discussed in Section 4.1.1), this implies that siderite does not fit the pattern for rhombohedral carbonates as shown in Fig. 5. Unsurprisingly, there is no apparent relationship

[2] The smaller $\delta^{18}O$ shift coincided with the lack of melt formed during laser-assisted fluorination of the solid oxide. A similar finding was observed during fluorination of one of the strontium oxide grains.

between the magnitude of $\Delta'^{17}O$ in the solid oxides and the corresponding $\delta^{18}O$ value. For completeness, this is shown in Fig. 6.

A puzzling feature of the relationship illustrated in Fig. 5 is that, for several of the carbonate minerals, it has been documented that the crystallographic form changes at elevated temperature. Aragonite undergoes transformation to the calcite structure at ~ 480–500 °C (Rao et al., 1975; Yoshioka and Kitano, 1985; Okumura et al., 2018), with the actual temperature varying with the nature and amount of impurities present. The presence of small amounts of Sr stabilises the aragonite phase, whereas biogenic examples usually transform to calcite at lower temperatures (Yoshioka and Kitano, 1985). The phase transition occurs at lower temperatures than required for the commencement of thermal decomposition, so it is feasible that the aragonite specimen heated in our investigation may have fully transformed to calcite before any release of CO_2 occurred. However, during TGA/EGA analysis, maximum CO_2 release was at 652 °C, lower than the 687 °C observed for the calcite example at the same heating rate. Furthermore, the $\Delta'^{17}O$ values of the resulting CaO were different.

The two most thermally stable carbonates included in this investigation, $BaCO_3$ and $SrCO_3$, are also known to transform at high temperature to rhombohedral structures. The respective transitions (for the pure compounds) have been reported as occurring at 803 °C (Okumura et al., 2018; Arvanitidis et al., 1996) or 806 °C (Lander, 1949) in $BaCO_3$ and at 912–924 °C (Rao et al., 1975; Lander, 1951) in $SrCO_3$. These transformations have been attributed to the onset of rotational disorder in the CO_3^{2-} ions (Lander, 1951). $BaCO_3$ additionally undergoes a higher temperature transformation, at 964–976 °C (Okumura et al., 2018; Arvanitidis et al., 1996; Lander, 1951), to a cubic (halite) structure, cation coordination number 8.

Conversely, quantum chemical modelling of the thermal decomposition of magnesite have shown that a structural phase transition from the rhombohedral form to a chiral orthorhombic structure occurs during the thermal decomposition process (Zhao et al., 2015).

For the aragonite group carbonates, the mean C–O distance and O–C–O bond angle increase linearly with unit cell volume, whereas the aplanarity of the CO_3^{2-} group (defined by the distance of

the C atom from the plane formed by the three O atoms) decreases (Antao and Hassan, 2009). The CO_3^{2-} group thus becomes more symmetrical (C–O distances nearly equal) and less aplanar as the cation radius increases, i.e. in the progression Ca < Sr < Pb < Ba (aragonite to witherite). Thus, the aragonite structure is the most distorted, whereas that of witherite is the least distorted, in terms of the geometry of the CO_3^{2-} group (Antao and Hassan, 2009).

Of the nine elements represented as cations in the various carbonate specimens used for this investigation, we note that only one is monoisotopic (^{55}Mn). Furthermore, the nucleus has non-zero spin (5/2). The two stable isotopes of copper, ^{63}Cu and ^{65}Cu, also have spin-active nuclei (3/2). All the other cations have more than two stable isotopes; furthermore, spin-active nuclei are present at only minor or trace abundances, as shown in Table A.2, compiled from literature data. The relatively large difference between the Δ'^{17}O values of MnO and CuO formed from thermal decomposition of the respective carbonates (as shown in Fig. 5) indicates that the abundance of spin-active nuclei in the metal cation is not influential in determining the Δ'^{17}O value of the metal oxide.

5.2. Non-photochemical processes associated with anomalous Δ'^{17}O values

Only a small number of non-photochemical processes that generate mass-independent oxygen isotopic distributions have been reported. Thermal dissociation of ozone at 110 °C (Wen and Thiemens, 1991) is one example, with the ^{17}O/^{16}O and ^{18}O/^{16}O ratios changing by an equal amount. Perhaps the most surprising finding is that reported by Sun and Bao (2011a, 2011b), who showed that the diffusion, at low pressure, of molecular O_2 gas in a closed volume defies mass-dependent isotopic distributions when a thermal gradient is applied. It was postulated (Sun and Bao, 2011b) that a – usually negligible – nuclear spin effect on the gas diffusion coefficient may be largely responsible, amplified by the temperature gradient. As noted by those authors, such an effect had been predicted from theoretical considerations some 35 years earlier (Zel'dovich and Maksimov, 1976). We are unconvinced, however, by the suggestion (Sun and Bao, 2011a; 2011b) that their finding may be relevant to explaining the isotopic anomaly generated by thermal decomposition of calcium and magnesium carbonates. In the carbonate decomposition experiments, the gaseous product CO_2 was

continuously removed by vacuum pumping, or by cryogenic trapping to effect complete and quantitative gas transfer.

5.3. The thermal decomposition mechanism – overview

Whereas there have been numerous investigations of the thermal decomposition of divalent metal carbonates (especially of calcite) over many decades, details of the mechanism remain largely conjectural. Recent quantum chemical modelling of the thermal decomposition of calcite (Zhao et al., 2013) and magnesite (Zhao et al., 2015), involving detailed potential energy surface calculations, have explored the relative feasibility of different reaction pathways. These theoretical studies provide valuable information towards elucidating the decomposition mechanism at the molecular level. By comparing activation energy barriers and rate constants with experimental results, the energetically most favourable route was identified in both cases. When combined with relevant kinetic studies (Wang et al., 2017), the decomposition was shown to be consistent with a multi-step process and the identity of intermediate and metastable phases suggested. Much remains to be understood, however. The occurrence of a 'mass independent' oxygen isotopic fractionation during the thermal decomposition process provides further clues to establishing the details of the process.

In crystalline solids, it is excitations of low energy phonons across the Brillouin zone that determine the thermal free energies and thus isotopic fractionation factors. *Ab initio* calculations require that the three-dimensional potential energy surface be defined, and at sufficiently high resolution to discriminate between different isotopes. This is impractical, as the associated computational requirements are too demanding. Furthermore, even if such a task was achievable, it has been shown that dissociation pathways do not always proceed via the 'saddle point' transition state on the potential energy surface. The first such report was on formaldehyde decomposition (Townsend et al., 2004), where a second trajectory was identified: this involved one H atom nearly detaching via the (energetically favourable) H + HCO channel, but lacking sufficient energy for complete dissociation. The H atom 'roamed' far from the main reaction path on the potential energy surface until it abstracted the other hydrogen atom, yielding vibrationally excited H_2 and rotationally

'cold' CO. Since that seminal discovery, numerous other examples of 'roaming' reactions have been identified. In a recent review (Suits, 2020), it was noted that the phenomenon has become recognised as being quite common, especially in unimolecular dissociations. Typically, the process involves near-dissociation of a quasi-bound system to radical fragments, followed by reorientation at long range and intramolecular abstraction. This can lead to the formation of unexpected reaction products, amongst other characteristics. We are not aware, however, that 'roaming' during the decomposition of any crystalline solid has been investigated, to date.

Three processes which might be implicated in the unusual fractionation of oxygen triple-isotopes during carbonate thermal decomposition are:

- A particular combination of mass-dependent processes, or a kinetic process involving an unusual θ value (although explicable by established theory);
- Fermi resonance occurring during carbonate vibrational modes at the temperature of incipient decomposition and coincidentally leading to enhancement of the abundance of ^{17}O in the released CO_2;
- A mechanism based on the magnetic isotope effect, but differing from that proposed by Buchachenko (2013).

We now consider these possibilities, in turn.

5.3. Could the ^{17}O anomaly result from one or more mass-dependent processes?

It has been recognised for many years, from $\delta^{18}O$ measurements, that thermal decomposition of carbonates is associated with a kinetic isotope effect (Sharma and Clayton, 1965). Cartigny et al. (2012) suggested that the oxygen isotope anomaly reported by Miller et al. (2002) might be the result of a fortuitous combination of equilibrium exchange and kinetic fractionation processes, characterised by mass-dependent fractionation laws with different θ values, such that the combined effect is to mimic a mass-independent fractionation process across a wide range of isotopic compositions. The idea was illustrated schematically by Cartigny et al. (2012). Such a combination does seem implausible, however, as was subsequently acknowledged (Eiler et al., 2013). More recently, Yeung

and Hayles (2021) argued, from a consideration of transition state theory, that θ_{A-B} values associated with kinetic fractionation of oxygen triple-isotopes in chemical processes (reactant A → products B) are actually not bounded by any limits, in principle, and therefore may exceed the 0.5305 maximum that applies to equilibrium exchange. The authors noted that the range of reported values, both measured and calculated, is therefore surprising; the absence of 'anomalous' kinetic θ_{A-B} values suggests that bounds on its value are 'imposed by chemical and not mathematical' limits. Yeung and Hayles (2021) suggested that the lower zero-point energy of isotopically substituted reactants may mitigate against the expression of anomalous reduced partition function ratios of the transition state values as anomalous kinetic isotope effects.

The only other report we are aware of in which oxygen triple-isotope fractionation during mineral thermal decomposition was investigated is that by Clayton and Mayeda (2009). In their study, the magnesian minerals brucite and serpentine, $Mg(OH)_2$ and $Mg_3Si_2O_5(OH)_4$ respectively, were thermally dehydrated in vacuum. Following brucite dehydration, conducted at 300°C, the $\delta^{18}O$ value of the released water was found to be about 15 ‰ lower than the brucite, whereas the MgO (periclase) also formed was correspondingly enriched in ^{18}O. The brucite, periclase and released water fitted a fractionation line of slope 0.503 on a $10^3\ln(1 + \delta^{17}O)$ versus $10^3\ln(1 + \delta^{18}O)$ plot[3]. For serpentine dehydration, conducted in steps from 100 to 600°C, a slope of 0.507 was obtained. These values are within the range for (mass-dependent) kinetic fractionation processes in the triple-isotope system as described by Young et al. (2002). We note that brucite dehydration essentially involves proton transfer between OH^- groups; it has been shown (Liu et al., 2018) to fit a first-order single reaction model for the main step (300–400 °C), whereas the diffusion of water molecules dominates at higher temperatures. This is accordingly quite different from the thermal decomposition of carbonates. Furthermore, unless the transition state in the carbonate thermal decomposition mechanism can be shown to cause such very different triple-isotope fractionation behaviour from that of the Young et al.

[3] A noted by Clayton and Mayeda (2009), their correction for the significant 'tailing' of the *m*/*e* 32 ion beam into the *m*/*e* 33 collector may have been an underestimate, in which case the true values of the reported slopes would have been slightly greater.

(2002) kinetic model, leading to predicted kinetic θ_{A-B} values of ~0.60 or greater, it seems unlikely that our findings can be explained by such a possibility.

5.4. Fermi resonance

Fermi resonance may occur when a diatomic or polyatomic vibrational energy level occurs at a frequency which is close to a multiple of the frequency of a different vibrational mode, rendering the two levels 'coincidentally degenerate'. In CO_2, for example, the υ_1 vibration at 1337 cm^{-1} is close to twice υ_2 at 667cm^{-1}. As a consequence, the 1337 cm^{-1} band (Raman active) is split. Fermi resonance thus causes shifting of the energies and intensities of absorption bands, which will be affected by isotopic substitution. In an FT-Raman and infrared spectroscopic study of aragonite-strontianite ($Ca_xSr_{1-x}CO_3$) solid solution (Alía et al., 1997), it was suggested that infrared spectral data were consistent with an overtone $2\upsilon_4$ band being in Fermi resonance with the corresponding υ_3 fundamental.

In calcite, υ_3 occurs at 1432 cm^{-1}, which is very close to twice the υ_4 frequency of 714 cm^{-1}. Similarly, in strontianite, twice the frequency of the υ_4 line at 704 cm^{-1} is close to the υ_3 line at 1400 cm^{-1}. In cerussite, the corresponding values are 685 cm^{-1} and 1369 cm^{-1}. The positions of the infrared and Raman bands for a free carbonate group, together with those for calcite and the orthorhombic carbonates aragonite, strontiantite, witherite and cerussite, are illustrated in Fig. 31 of Speer (1983). Depending on whether or not there is a linear progression in vibrational energy levels associated with substituting ^{16}O by ^{17}O or ^{18}O in the metal carbonate could have significant implications for the isotopic composition of the thermal decomposition products, if the reaction pathway is influenced by Fermi resonance. Such a hypothesis would require, however, not only a non-linear energy progression associated with oxygen isotope substitution, but also that Fermi resonance occurs during vibrational excitation at the temperatures of thermal decomposition of all the metal carbonates we investigated. This seems unlikely for aragonite, from the positions of the υ_1 to υ_4 infrared and Raman bands (Speer, 1983). The question of whether Fermi resonance is influential in determining the oxygen triple-isotope compositions of the carbonate decomposition products – and for all the carbonates used for

this study – remains unresolved. However, a potentially promising way forward is discussed in Section 5.8.

5.5. The Magnetic Isotope Effect and evaluation of the Buchachenko (2013) hypothesis

The occurrence of the magnetic isotope effect was postulated by Lawler and Evans (1971), although initially its magnitude was considered to be negligible. It involves the formation of an ion-radical pair, the lifetime of which is sufficient for hyperfine coupling between spin-active nuclei and unpaired electrons to influence interconversion between the electronic singlet and triplet states of the pair. Such spin-state mixing changes the proportion of reactive intermediates that can participate in spin-selective reactions. Empirical findings compatible with such a mechanism were described by Buchachenko et al. (1976). During the following four decades, numerous other examples have been documented, involving spin-active nuclei of various elements (Buchachenko and Lawler, 2017). Salikhov (1996) gives a comprehensive introduction to the concept and theory. Unlike the nuclear field shift effect, which acts both at equilibrium and in kinetically hindered reactions (by changing activation energies in the latter case), magnetic isotope effects are purely kinetic, affecting the rates of formation and branching ratios of possible reaction products (Dauphas and Schauble, 2016).

Whereas most investigations of the magnetic isotope effect have involved radical pair reactions in the liquid phase (notably in solution) and have established a strong viscosity dependence that mediates the lifetimes of the cage radicals, solid state examples have been documented. For example, Turro et al. (1985) showed that partial photolysis of solid dibenzyl ketone adsorbed on porous silica generates anomalous enrichment of ^{17}O and ^{13}C in the residual ketone. Silicon oxidation by oxygen (Koplak et al., 2013) provides another example, with ^{29}Si (nuclear spin 1/2, nuclear magnetic moment 0.555) being oxidised twice as rapidly as ^{28}Si and ^{30}Si. It is worth also highlighting that magnetic field effects, which also share essentially the same mechanism of spin-state mixing in spin-correlated radical pairs and spin-selective reaction, are numerous and have been well studied in many solid state reactions. In such cases, electrons and ‘holes’ migrate, rather than the radicals themselves, and are often referred to as bipolaron pairs.

The Buchachenko (2013) hypothesis to explain the ^{17}O anomaly associated with thermal decomposition of divalent metal carbonates is based on carbonate decomposition proceeding via thermal generation of a short-lived ion-radical pair in the singlet spin-state, with the metal ion being reduced to univalency. With calcium as the cation, for example,

$$Ca^{2+}\,CO_3^{2-} \rightarrow (Ca^{+}\,CO_3^{-\bullet})^{S} \quad (8)$$

In the case of ^{17}O, this singlet born radical pair can undergo coherent singlet-triplet spin-state mixing to generate the triplet radical pair, driven by the hyperfine coupling to the ^{17}O nucleus (while this does not occur in zero applied magnetic field in the case of ^{16}O or ^{18}O, as those nuclei have zero spin).

$$(Ca^{+}\,{}^{17}OCO_2^{-\bullet})^{S} \leftrightarrow (Ca^{+}\,{}^{17}OCO_2^{-\bullet})^{T} \quad (9)$$

Back electron transfer to regenerate the carbonate is spin-selective, taking place only from the singlet state radical pair:

$$(Ca^{+}\,CO_3^{-\bullet})^{S} \rightarrow Ca^{2+}\,CO_3^{2-} \quad (10)$$

$$(Ca^{+}\,CO_3^{-\bullet})^{T} \not\rightarrow Ca^{2+}\,CO_3^{2-} \quad (11)$$

Buchachenko considers the forward reaction of triplet pairs in which the $CO_3^{-\bullet}$ anion-radical undergoes fast β-scission of a C–O bond as follows:

$$(Ca^{+}\,{}^{17}OCO_2^{-\bullet})^{T} \rightarrow {}^{17}OCO + (Ca^{+}\,O^{-\bullet})^{T} \quad (12)$$

Back electron transfer in the $Ca^{+}\,O^{-\bullet}$ generates the oxide product. Buchachenko implies that all singlet radical pairs will re-combine and all triplet radical pairs will produce the oxide product. A more detailed presentation would also include the fact that the product can be formed from the singlet state radical pair and that this reaction also competes with back electron transfer:

$$(Ca^{+}\,{}^{17}OCO_2^{-\bullet})^{S} \rightarrow {}^{17}OCO + (Ca^{+}\,O^{-\bullet})^{S} \quad (13)$$

However, this subtlety only qualitatively reduces the size of the effect and is not problematic for the mechanism. Nevertheless, it is important to recognise that, in this proposed mechanism, reaction (13) represents the only decomposition channel for those carbonate anion radicals which contain no

^{17}O. It is the spin-selective back electron transfer to the carbonate that is important in determining the differing reactivity of singlet and triplet radical pairs.

Note that the 'forbidden' route of back electron transfer from the triplet state radical pair in step (12), which would re-generate $CaCO_3$, means that the overall lifetime of the radical pair is increased. Under conditions of continuous radical pair formation (as we have here), the concentration of radical pairs at any given time increases, leading to an increased production rate of $C^{17}OO$, $CO^{17}O$ and $Ca^{17}O$. The presence of ^{17}O 'switches on' coherent S-T mixing, which reduces regeneration of the original $CaCO_3$ from back electron transfer. Thus, the overall decomposition is faster than for the ^{18}O-containing isotopomer. In the latter, some pairs now become triplet; these are more likely to react rather than re-generate $CaCO_3$.

Finally, Buchachenko concludes that reaction (12) will cause the CO_2 to become anomalously enriched in ^{17}O whereas the $Ca^{2+}\,O^{2-}$ becomes correspondingly depleted. At first sight, this mechanism seems plausible. However, more careful inspection reveals that it is actually incapable of explaining our experimental observations. The problem lies in step (12) and is an artefact of ordering the symbols in a particular way, implying that somehow in the triplet reaction channel, ^{17}O will only be present in the carbon dioxide formed, not in the metal oxide. Step (12) actually represents three different possibilities:

$$(Ca^{+}\,{}^{17}OCOO^{-\bullet})^{T} \rightarrow {}^{17}OCO + (Ca^{+}\,O^{-\bullet})^{T} \qquad (14)$$

$$(Ca^{+}\,OC^{17}OO^{-\bullet})^{T} \rightarrow OC^{17}O + (Ca^{+}\,O^{-\bullet})^{T} \qquad (15)$$

$$(Ca^{+}\,OCO^{17}O^{-\bullet})^{T} \rightarrow OCO + (Ca^{+}\,{}^{17}O^{-\bullet})^{T} \qquad (16)$$

All three radical pairs are identical and so would undergo singlet-triplet state mixing at the same rate. The mechanism does not propose that these subsequent reactions show any difference in rate (i.e., they are not spin-selective steps) and therefore the proposed mechanism does not lead to any ^{17}O enrichment in the CO_2 or depletion in the $Ca^{2+}\,O^{2-}$. The triplets in reactions (14) to (16) could all be replaced by the corresponding singlet states, and all occurrences of ^{17}O replaced by ^{18}O, yet these

three reactions would still take place at the same rate (neglecting any kinetic isotope effect), as this is a two-electron spin-independent process.

Does the Buchachenko mechanism still predict a MIE? The answer is 'yes', it predicts that singlet-triplet state mixing takes place in the ^{17}O-containing carbonate isotopomer, but not in the other isotopomers. This implies that, during thermal decomposition, carbonate containing ^{17}O will decompose faster than carbonate which does not contain ^{17}O. The effect of this would be that, after partial decomposition, the resulting metal oxide and carbon dioxide would *both* be relatively enriched in ^{17}O, whereas the residual carbonate would be correspondingly depleted in ^{17}O. However, if carbonate decomposition proceeds to completion (as in our experiments), neither of the decomposition products would contain a ^{17}O anomaly, regardless of whether or not singlet-triplet mixing had taken place (i.e. there would be no evidence of MIE involvement). The mechanism proposed by Buchachenko (2013) therefore cannot be a correct description of the thermal decomposition of any of the carbonates we investigated, as its 'true' outcome is not in accord with our experimental findings.

5.6. A new MIE-based explanation of the ^{17}O anomaly

What is clear from the problem with the Buchachenko mechanism is that, in order to have a radical pair-based mechanism that causes the observed oxygen triple-isotope distributions in the two reaction products, the spin-state mixing rate must differ between radical pairs that can selectively generate these two products. Additionally, there are two further key features that any plausible mechanism must possess. The first is that the mechanism must generate a difference in yield of products in which the ^{17}O appears (the metal oxide or the carbon dioxide), rather than just a difference in their rates of production. The second is that the mechanism must also be able to explain how the radicals in the pair become sufficiently separated such that the electron exchange interaction becomes similar to – or negligible – relative to the size of the hyperfine coupling. This condition is necessary to observe coherent radical pair spin effects. We propose a new radical pair-based mechanism that fulfils these criteria and predicts ^{17}O enrichment in the carbon dioxide and depletion

in the metal oxide, consistent with the experimental findings and the magnetic properties of the proposed intermediate radicals. We then consider the plausibility of this mechanism, based on other studies of the mechanism of carbonate decomposition and the results of magnetic field effect measurements. Finally, we propose a diagnostic test.

The first important postulate of the mechanism is that, when strongly heated, the carbonate ions are vibrationally excited and capable of undergoing vibrational dissociation. For this to have any consequence, however, there must be somewhere in the lattice structure for one of the resulting fragments to move to, otherwise the energy is distributed and the bond reforms. Thus, the first step of the mechanism is to consider the diffusion of defect sites in the crystalline lattice to a position adjacent to the dissociating carbonate ion. With a lattice vacancy available, we propose that the carbonate ion undergoes homolytic cleavage of one of the C–O bonds, generating a radical pair which consists of $O^{-\bullet}$ and $CO_2^{-\bullet}$. As the carbonate ion remains in the singlet ground electronic state (the temperature is not high enough for significant electronic excitation), the radical pair is generated in the singlet state:

$$CO_3^{2-} + \text{‘vacancy site’} \rightarrow (O^{-\bullet}\, CO_2^{-\bullet})^{S} \quad (17)$$

If neither member of the radical pair contains ^{17}O, no hyperfine coupling is possible and so, in zero field, no coherent spin-state mixing to the triplet state of the radical pair can occur. The fate of such radical pairs is either to re-form the carbonate ion, or for electron transfer to take place from the $CO_2^{-\bullet}$ to $O^{-\bullet}$, generating the metal oxide and carbon dioxide. The CO_2 then diffuses through the lattice and escapes once it reaches the surface. However, if the carbonate ion contains ^{17}O, there are now three possible arrangements, leading to two different radical pairs by reaction (17):

$$^{17}OCOO^{2-} \rightarrow (^{17}O^{-\bullet}\, COO^{-\bullet})^{S} \quad (18)$$

$$OC^{17}OO^{2-} \rightarrow (O^{-\bullet}\, C^{17}OO^{-\bullet})^{S} \quad (19)$$

$$OCO^{17}O^{2-} \rightarrow (O^{-\bullet}\, CO^{17}O^{-\bullet})^{S} \quad (20)$$

The radical pairs produced by reactions (19) and (20) are identical. As above, both radical pairs can undergo bond reformation from the singlet state only, to regenerate the original carbonate:

$$(^{17}O^{-\bullet}\ CO_2^{-\bullet})^{S} \rightarrow {}^{17}OCOO^{2-} \quad (21)$$

$$(O^{-\bullet}\ C^{17}OO^{-\bullet})^{S} \rightarrow OC^{17}OO^{2-} \quad (22)$$

which can dissociate again via any of reactions (18) – (20). This step is critical, as it allows conversion between the two types of radical pair, which is necessary for a yield effect rather than solely a kinetic effect. Also, as above, electron transfer (which is also spin-selective, occurring only from the singlet state) can generate the reaction products:

$$(^{17}O^{-\bullet}\ CO_2^{-\bullet})^{S} \rightarrow {}^{17}O^{2-} + \ CO_2 \quad (23)$$

$$(O^{-\bullet}\ C^{17}OO^{-\bullet})^{S} \rightarrow O^{2-} + \ C^{17}OO \quad (24)$$

However, in the ^{17}O case, these radical pairs can both undergo coherent spin-state mixing to the triplet state, due to the hyperfine coupling to the ^{17}O:

$$(^{17}O^{-\bullet}\ CO_2^{-\bullet})^{S} \leftrightarrow (^{17}O^{-\bullet}\ CO_2^{-\bullet})^{T} \quad (25)$$

$$(O^{-\bullet}\ C^{17}OO^{-\bullet})^{S} \leftrightarrow (O^{-\bullet}\ C^{17}OO^{-\bullet})^{T} \quad (26)$$

Whereas it may be possible from the triplet state of these radical pairs for the $CO_2^{-\bullet}$ to revert back to its original oxide partner and become trapped there if the vacancy escapes (and ultimately to regenerate the carbonate ion after spin relaxation), the electron transfer is spin-forbidden. As a result, the triplet radical pair cannot generate the decomposition products. Fig. 7 shows the overall kinetic scheme with no isotope distinction, whereas Fig. 8 provides an exhaustive representation in the case of ^{17}O, to highlight the two different possible radical pairs.

The critical steps, then, are the singlet-triplet mixing reactions (25) and (26) and the spin selective forward electron transfer reactions, (23) and (24). The latter occur at the same rate, so the MIE arises due to a difference in the efficiency of the coherent spin-state mixing in reactions (25) and (26). If (25) is more efficient than (26), then the $(^{17}O^{-\bullet}\ CO_2^{-\bullet})$ radical pair will be more likely to undergo spin-state mixing and less likely to proceed to products than the $(O^{-\bullet}\ C^{17}OO^{-\bullet})$ pair. This would lead to the carbon dioxide being enriched in ^{17}O and the metal oxide being depleted. If (26) is faster than (25), then the opposite is true, and the carbon dioxide will be depleted in ^{17}O, whereas the metal oxide will be enriched.

Based on the experimental findings, for this mechanism to be correct, the spin-state mixing in the ($^{17}O^{-\bullet}$ $CO_2^{-\bullet}$) radical pair should be faster than in the ($O^{-\bullet}$ $C^{17}OO^{-\bullet}$) pair, which suggests that the hyperfine coupling to ^{17}O in the $^{17}O^{-\bullet}$ radical ion should be greater than the hyperfine coupling in the $C^{17}OO^{-\bullet}$ radical. It might be anticipated that this would be true, given that, in the $C^{17}OO^{-\bullet}$ radical, the electron is delocalised and thus has less spin density on the ^{17}O atom than in $^{17}O^{-\bullet}$, although the 's' character of the orbitals involved is also very important. In practice, this can be confirmed by existing measurements and calculations to determine the ^{17}O hyperfine coupling in these two species. Blondel et al. (2001) determined the hyperfine structure of the $^{17}O^{-\bullet}$ radical ion, using photodetachment microscopy, as 151 MHz (5.4 mT), whereas Chiesa and Giamello (2007) measured the ^{17}O hyperfine hyperfine coupling[4] in the $C^{17}OO^{-\bullet}$ radical to be 102.2 MHz (3.7 mT), from EPR spectra of this radical on the surface of MgO. The correct relative magnitudes, together with the fact that both proposed radical species have been observed experimentally, provides credible support for our proposed mechanism.

Strong support for such a mechanism is provided by its compatibility with recent studies of the thermal decomposition of calcite (Zhao et al., 2013; Wang et al., 2017; Li et al., 2018) and magnesite (Zhao et al., 2015). In these investigations, the decomposition mechanism was found to proceed via the reaction sequence (using $MgCO_3$ as the example; Zhao et al., 2015):

$$MgCO_3 \rightarrow (MgO)CO_2 \rightarrow \ MgO + CO_2 \qquad (27)$$

The authors used quantum chemical calculations to examine the energies of the different possible intermediate geometries after cleavage of the one of the carbonate C–O bonds, to generate the intermediate indicated in reaction (27). Their findings are consistent with the formation of a radical

---

[4] Hyperfine coupling constants are reported in the literature as a frequency (usually in MHz) or magnetic flux density (usually in milliTesla or Gauss, where 1 mT ≡ 10 G). Conversion between MHz and mT values is given by the Larmor precession relationship:

$f = 10^{-9} \frac{g\mu_B}{h} B$ where μ_B is the Bohr magneton, g is the hyperfine coupling value and h is Planck's constant.

Substitution of numerical values, with g for a free electron, gives, for a magnetic flux density of 1 mT, a frequency of: $(10^{-9} \times 2.00232 \times 9.27401 \times 10^{-24}) / (6.62607 \times 10^{-34}) = 28.025$ MHz .

pair via homolytic cleavage, as we propose. As discussed in those papers, the decomposition of calcite and magnesite (and, by extension, the other metal carbonates under consideration) proceeds via a complex mechanism which involves chemical bond breaking, lattice destruction and formation and absorption, desorption and diffusion of gaseous products, among other complications (Zsakó, 1968). Our proposed mechanism represents a simple overview of the chemical reaction occurring and, while relying on the generation or movement of lattice vacancies, does not address the detailed mechanism of how the lattice changes or how the carbon dioxide moves through and escapes from it. However, if our proposed MIE mechanism is indeed the correct explanation of our experimental measurements, then it carries some broad implications for the decomposition mechanism.

5.6.1. Time and length scales for radical pair reactions

In order to manifest magnetic field and isotope effects, radical pair reactions must meet two key requirements. The first is that the individual components must separate to sufficient distances to allow hyperfine coupling-driven coherent spin-state mixing before spin-selective reaction. The second is that they must remain at these separations long enough for the spin-state mixing process to have a measurable effect. The former is due to the fact that the electron exchange interaction, which drops very rapidly with the separation of the members, completely overwhelms the hyperfine coupling and stops coherent spin-state mixing when the radicals are close together. Typically, radical pair constituents need to be at least 5-8 Å apart in order for appreciable spin-state mixing to be possible (and even further apart for optimal mixing). In the case of the latter, based on publications mentioned above, the difference in hyperfine coupling of the two radicals is of the order of 50 MHz (1.8 mT) which, given that the nuclear spin of ^{17}O is 5/2, requires the radical pair lifetime to be of the order of nanoseconds to tens of nanoseconds, in order to produce an appreciable difference between the pairs. Both these facts are accounted for by the need for lattice vacancies to allow the C–O bond dissociation to take place completely and generate a separated radical pair, allowing spatial configurations where the spin-state mixing is possible and where back electron transfer to form products is still sufficiently rapid. One can imagine other variants of this general mechanism, which

cannot easily be distinguished on the basis of an isotope effect alone. For example, the process might be restricted to being a surface effect, with bond-breaking occurring on the lattice surface rather than in an embedded vacancy. Such intricacies are beyond the scope of this initial mechanistic proposal.

In order to confirm that the mechanism highlighted in Fig. 8 can produce the observed isotope effect, simple kinetic simulations were performed in which spin-state mixing was treated approximately as a simple, first-order rate process, with a rate coefficient equal to the hyperfine coupling (in frequency units). These simulations – using code written in MATLAB™ – were performed by expressing the reaction scheme in Fig.8 as a series of first order linear differential equations in matrix form and using matrix exponentiation to obtain the time propagator. The time dependence of the principal species was then determined, using a time step of 1 ns. The simulations produced a clear yield effect on the reaction, resulting in ^{17}O enrichment in the CO_2, consistent with the experimental findings. Fig. 9 shows an example simulation for a particular set of kinetic parameters. Depending on the various rate coefficients, the magnitude of the enrichment can be controlled and the overall rate matched to the actual decomposition timescale.

5.6.2. Experiments to test a MIE based mechanism and their consequences for this new mechanism

As discussed above (in Sections 1, 3.3.1, 4.1.1 and 4.1.2 respectively), two specific experiments were undertaken to test the Buchachenko MIE mechanism. The first was the oxygen isotopic measurements on copper (II) carbonate thermal decomposition products. In the Buchachenko mechanism, one radical pair member is the metal cation in univalent state. In the case of Cu^+, this has no unpaired electron and thus the Buchachenko mechanism predicts that the MIE should not occur in this particular example. In the new mechanism, however, no univalent metal ion is formed and the metal cations are not generally involved directly in the steps of the decomposition reaction. On this basis, there is no reason to suggest that the anomalous isotope effect would be different in the case of copper (II) carbonate thermal decomposition, which is consistent with the experimental findings. The potential influence of the divalent metal ion in our proposed mechanism is discussed below.

The second experiment undertaken to provide insight into the possibility of an MIE-based mechanism was to investigate the effect of an applied magnetic field of ~ 0.25 T during the thermal decomposition reaction, using siderite as the carbonate example. Applying the magnetic field produced no effect on the oxygen triple-isotope ratios in the resulting FeO. However, it is worth highlighting that, in all the other experiments conducted for this investigation (with no magnetic field applied), samples would still have experienced a local magnetic field, generated by the electrical current flowing through the helical heating coil of the surrounding tube furnace. The upper limit of the magnitude of this magnetic field is estimated to have been about 3 mT, at the highest temperatures.

We note that some of the experiments discussed in the initial report (Miller et al., 2002) were performed using an infrared (10.6 μm) laser instead of a heating coil for the carbonate heating process; this would have been associated with a magnetic field much closer to zero. In those experiments, which involved carbonates of Ca and Mg only, anomalous ^{17}O depletion occurred in the resulting metal oxides, but to a lesser extent than when using a tube furnace as the heat source. The observed difference may or may not be significant in the present context. An additional complication is that the laser heating was conducted over a much shorter period (1–2 hours, rather than several days as when heating by tube furnace), which was probably influential. In summary, a ^{17}O anomaly was produced in all the carbonate thermal decomposition experiments, regardless of whether the heating was conducted in (almost) zero magnetic field, or in fields of a few mT, or ~250 mT.

In the case of the new mechanism, there are three different mechanisms that may be important to consider for magnetic fields in the range of 0 to 0.25T. The first is the electron Zeeman effect. It can be considered – to a first approximation – that an applied magnetic field would serve to reduce the spin-state mixing efficiency by two-thirds in the radical pairs. In zero field, the singlet state can mix with all three triplet states whereas, in high field, two of the triplet states are energetically inaccessible due to the electron Zeeman effect. Secondly, there might be an opposite effect of increasing the spin-state mixing efficiency at weaker fields, due to the so-called low field effect (LFE) (Woodward, 2002; Timmel and Henbest (2004)). The third possible effect might be manifest due to an increase in spin-

state mixing resulting from more rapid mixing between the S and T_0 states due to a difference in g-values of the two radicals comprising the pair. The difference in g-values will be identical for the two different radical pairs and so will give an equal increase in the S–T_0 mixing rate for both radical pairs; this could also influence the size of the observed MIE. Typical g-values for oxygen-centred radicals are somewhat larger than for typical carbon-centered radicals and, if large enough, this might be able to influence the size of the MIE at magnetic fields of 250mT and more. It is clear from the complexity and overlapping nature of these mechanisms that it is difficult to predict how an applied magnetic field might influence the magnitude of the MIE without an appropriate simulation. In order to properly investigate the effect of an applied magnetic field on the magnitude of ^{17}O enrichment (or depletion), detailed spin-dynamic simulations have been conducted for this study, based on the kinetic model shown in Fig. 9. The details of these simulations are beyond the scope of this article and will be presented elsewhere. Early results, however, suggest that measuring the influence of an applied magnetic field in the range of a few tens of mT would increase the magnitude of the ^{17}O anomaly and would be a good diagnostic test for this new magnetic isotope effect-based mechanism.

Some of the metal cations (Cu^{2+}, Mn^{2+}, Fe^{2+}) have non-zero spin electronic ground states. This begs the question of whether this would influence the magnitude of the enrichment. Whereas paramagnetic ions may induce incoherent spin relaxation in the adjacent radical pairs through modulation of the dipolar interaction, the effect at zero field is not well understood. In addition, the magnitude of any influence will depend on the detailed kinetic parameters of the reaction and may be negligible. Therefore, without much more detailed information, it is difficult to make any reasonable prediction about the extent to which it might affect the proposed mechanism.

With regard to the potential effect of the crystallographic structure on the magnitude of the effect, this may influence the availability and separation of vacancies which could potentially influence the size of the observed effect, but any clear correlation would require a much more detailed picture of vacancy behaviour in these materials as decomposition takes place.

5.7. Cosmochemical implications

Thermal decarbonation of carbonates in nature, despite occurring on a large scale at subduction zones and during high grade metamorphism in the Earth's crust, invariably proceeds under conditions which facilitate oxygen isotope exchange with hydrous fluids or melts. Therefore, any anomalous ^{17}O depletion in the condensed phase would be transient. However, our findings may be of relevance in a cosmochemical context. The reported detection of calcite associated with amorphous silicates in two planetary nebulae (Kemper et al., 2002) and protostars (Ceccarelli et al., 2002; Chiavassa et al., 2005) devoid of planetary bodies, together with the experimental demonstration that carbonates can be formed with amorphous silicates during the non-equilibrium condensation of a silicate gas in a H_2O-CO_2-rich vapour (Toppani et al., 2005), suggests that thermal processing of such material may provide a mechanism for the mass-independent fractionation of oxygen isotopes in protoplanetary systems. We note that the magnitude of the change in $\Delta'^{17}O$ associated with the transition from carbonate to divalent metal oxide, as reported above, is of the order of the $\Delta'^{17}O$ difference between bulk silicate Earth and Mars; the latter is characterised by a $\Delta'^{17}O$ value of 0.305 ± 0.004 ‰, standard error (Franchi et al., 1999), if reported using the definition of $\Delta'^{17}O$ (λ_{RL} = 0.524 and γ_{RL} = 0 in Eq. (6)) as adopted throughout this paper. For comparison, carbonate extracted from meteorite ALH84001, believed to be of Martian origin, is characterised by a $\Delta'^{17}O$ value of 0.74 ± 0.05 ‰ (recalculated from Farquhar et al., 1998).

In contrast to thermal processing of carbonates and with hyperfine coupling of ^{17}O postulated, Haberkorn et al. (1977) suggested that hyperfine modulated radical *recombination* may occur in a cosmochemical context on interstellar grain surfaces, leading to isotopic enrichment of spin-active isotopes such as ^{17}O in the molecules formed.

5.8. Suggestions for further investigation

For further investigation of the unusual isotope effect, reducing the $\Delta'^{17}O$ variations between replicate decompositions of the same carbonate mineral is a principal requirement. Use of a constant heating rate for all specimens, whilst continuing to minimise the potential for oxygen isotope

exchange between the thermal decomposition products, could improve data consistency and comparability. Thermal decomposition at constant heating rate in a helium flow (Sharp et al., 2003), with trapping of the evolved CO_2, may be an effective alternative to heating *in vacuo*. Such refinements, leading to more precisely defined $\Delta'^{17}O$ values, would strengthen – or refute – the apparent relationship between carbonate crystallographic structure and the magnitude of $\Delta'^{17}O$ in the thermal decomposition products. In addition, testing whether the magnitude of the isotopic anomaly in individual examples exhibits a magnetic field dependence when the flux density is a few tens of mT provides a means of validating (or refuting) the MIE-based hypothesis presented in this paper. Furthermore, a potentially definitive test for establishing whether or not radicals are generated during thermal decomposition of carbonates would be to conduct electron spin resonance (electron paramagnetic resonance) measurements during the heating process.

Future investigations might also include other divalent carbonate mineral examples, such as otavite ($CdCO_3$) and spherocobaltite ($CoCO_3$), both of which are rhombohedral; possibly laboratory reagent examples of other divalent metal carbonates too – for which triple-isotope measurements of the released CO_2 would be needed in addition to those of the metal oxide. Furthermore, although the cation is monovalent, Ag_2CO_3 decomposes readily to form the metal oxide and CO_2, at a lower temperature than divalent carbonate examples. Because Ag_2CO_3 is monoclinic, the oxygen triple-isotope fractionation pattern associated with its thermal could therefore be usefully compared with that of $CuCO_3$ decomposition, under identical experimental conditions. The $\Delta'^{17}O$ value of the resulting Ag_2O should be similar to that reported herein for CuO, if the $\Delta'^{17}O$ relationship with cation coordination number is as suggested from our findings.

Whether or not Fermi resonance occurs in the vibrational spectra of any of the carbonates included in our investigation, at the temperatures associated with thermal decomposition, is – as far as we are aware – unresolved. If it does occur, Fermi resonance might be expected to influence the oxygen triple-isotope compositions of the thermal decomposition products. The correct assignment of spectral features can be challenging, however, in experiments and simulations when double peaks are present,

because such peaks can have different origins. Fermi dyads are a common class of such doublets, stemming from resonance of the fundamental excitation of a mode with the overtone of another. A new approach to unambiguously characterising Fermi resonances in density functional theory (DFT) based simulations of condensed phase systems (Basire et al., 2017) suggests that spectral features can be confidently assigned and the two resonating modes identified. The application of such an approach to analysing the infrared and Raman spectra of carbonates at elevated temperatures, in conjunction with isotopic substitution modelling, offers a promising way forward to explore what role, if any, Fermi resonance has on the magnitude of $\Delta'^{17}O$ present in carbonate thermal decomposition products.

6. CONCLUSIONS

We have demonstrated that anomalous fractionation of $^{17}O/^{16}O$ relative to $^{18}O/^{16}O$ occurs during the thermal decomposition of all (eleven) divalent metal carbonate examples investigated, regardless of the cation identity. The magnitude of the anomaly, quantified as $\Delta'^{17}O$, ranged from –0.20 ‰ to –0.43 ‰ in individual samples of solid oxide, when λ_{RL} is assigned as 0.524 and when a protracted, controlled heating protocol was utilised. The actual magnitude of the anomaly is dependent on the experimental details. For thermal decomposition conducted under similar conditions, there appears to be a correlation between the magnitude of $\Delta'^{17}O$ in the solid oxide and the cation coordination number (at room temperature) in the parent carbonate. An explanation consistent with the empirical findings, and based on a newly-derived mechanism involving the magnetic isotope effect, is proposed. This has strong similarities to recent quantum chemical calculations of calcite and magnesite thermal decompositions. Further work is required to validate the proposed pathway. Finally, we cannot exclude the possibility that Fermi resonance might be contributing to the isotopic anomaly, in some of the examples investigated.

ACKNOWLEDGEMENTS

MFM gratefully acknowledges that co-author JRW identified the hitherto unrecognised problem with the Buchachenko (2013) mechanism and devised the alternative presented in this paper (as

contributed by JRW in Sections 5.5, 5.6 and Figs. 7–9). The idea that Fermi resonance might be involved in the unusual isotope effect was suggested to MFM by John R. Hulston (lead author of Hulston and Thode, 1965, cited in the text). PFM and MFM are grateful to Furio Cora (University College, London) for helpful consultations. MFM expresses appreciation to Open University colleagues Jenny M. Gibson for laboratory assistance and Andy G. Tindle for electron probe measurements of the natural carbonate specimens. Also to Alan Hart, for the provision of specimens from the mineral collection at the Natural History Museum, London. Finally, MFM thanks Anatoly Buchachenko for congenial discussions about the magnetic isotope effect.

SUPPLEMENTARY MATERIAL

Supplementary material for this article, providing the results of elemental and phase purity measurements of the natural carbonate minerals used in this investigation, is available in an online Electronic Annex at: https://doi.org/10.1016/j.gca.2021.xx.xxx.

REFERENCES

Alía J. M., Díaz de Mera Y., Edwards H. G. M., González Martín P. and Lópes Andrés S. (1997) FT-Raman and infrared spectroscopic study of aragonite-strontianite ($Ca_xSr_{1-x}CO_3$) solid solution. *Spectrochim. Acta A* **53**, 2347–2362.

Antao S. M. and Hassan I. (2009) The orthorhombic structure of $CaCO_3$, $SrCO_3$, $PbCO_3$ and $CaCO_3$: linear structural trends. *The Canadian Mineral*. **47**, 1245–1255.

Arvanitidis I., Sichen D. and Seetharaman S. (1996) A study of the thermal decomposition of $BaCO_3$. *Metallurg. Materials Trans. B*, **27B**, 409–416.

Basire M., Mouhat F., Fraux G., Bordage A., Hazemann J-L., Louvel M., Spezia R., Bonella S. and Vuilleumier R. (2017) Fermi resonance in CO_2: mode assignment and quantum nuclear effects from first principles molecular dynamics. *J. Chem. Phys*. **146**, 134102.

Bhattacharya S.K., Savarino J. and Thiemens M. H. (2000) A new class of oxygen isotopic fractionation in photodissociation of carbon dioxide: potential implications for atmospheres of Mars and Earth. *Geophys. Res. Lett.* **27**, 1459–1462.

Bhattacharya S. K. and Thiemens M. H. (1989) New evidence for symmetry dependent isotope effects: O + CO reaction. *Z. Naturforsch.* **44**, 435–444.

Bigeleisen J. and Goeppert-Mayer M. (1947) Calculation of equilibrium constants for isotopic exchange reactions. *J. Chem. Phys*. **15**, 261–267.

Bigeleisen J. and Wolfsberg M. (1957) Theoretical and experimental aspects of isotope effects in chemical kinetics. *Adv. Chem. Phys*. **1**, 15–76.

Blondel C., Delsart C., Valli C. and Yiou S. (2001) Electron affinities of ^{16}O, ^{17}O, ^{18}O, the fine structure of ^{16}O and the hyperfine structure of $^{17}O^-$. *Phys. Rev. A* **64**, 052504 (14pp).

Buchachenko A. L. (2013) Mass-independent isotope effects. *J. Phys. Chem. B* **117**, 2231–2238.

Buchachenko A. (2018) Magnetic isotopes as a means to elucidate Earth and environmental chemistry. *Russ. Chem. Rev.* **87** (8), 727–740.

Buchachenko A. L., Galimov E. M., Ershov V. V., Nikiforov G. A. and Pershin A. D. (1976) Isotope enrichment induced by magnetic interactions in chemical reactions. *Doklady Akademii Nauk SSSR* **228**, 379−382.

Buchachenko A. and Lawler R. G. (2017) New possibilities for magnetic control of chemical and biochemical reactions. *Acc. Chem. Res*. **50**, 877–884.

Cao X. and Liu Y. (2011) Equilibrium mass-dependent fractionation relationships for triple oxygen isotopes. *Geochim. Cosmochim. Acta* **75**, 7435–7445.

Cartigny P., Eiler J. M., Agrinier P. and Assayag N. (2012) On the mass independent fractionations of O, Hg, Si, Mg and Cd during open system evaporation or thermal decomposition. *Sixth Internatnl. Symp. Isotopomers (ISI 2012),* Washington DC, USA. p.26 (abstr.)

(https://www.yumpu.com/en/document/read/21466085/sixth-international-symposium-on-isotopomers-geophysical-)

Ceccarelli C., Caux E., Tielens A. G. G. M., Kemper F., Waters L. B. F. M. and Phillips T. (2002) Discovery of calcite in the solar type protostar NGC 1333-IRAS4. *Astron. Astrophys*. **395**, L29–L33.

Chakraborty S., Ahmed M., Jackson T. L. and Thiemens M. H. (2012) Experimental test of self-shielding in vacuum ultraviolet photodissociation of CO. *Science* **321**, 1328–1331.

Chiavassa A., Ceccarelli C., Tielens A. G. G. M., Caux E. and Maret S. (2005) The 90–110 mm dust features in low to intermediate mass protostars: calcite? *Astron. Astrophys*. **432**, 547–557.

Chiesa M. and Giamello E. (2007) Carbon dioxide activation by surface excess electrons: an EPR study of the CO_2^- radical ion adsorbed on the surface of MgO. *Chem. Eur. J*. **13**,1261–1267.

Clayton R. N. and Mayeda T. K. (1988) Formation of ureilites by nebular processes. *Geochim. Cosmochim. Acta* **52**, 1313–1318.

Clayton R. N. and Mayeda T. K. (2009) Kinetic isotope effects in oxygen in the laboratory dehydration of magnesian minerals. *J. Phys. Chem. A* 113, 2212–2217.

Coplen T. B., Kendall C. and Hopple J. (1983) Comparison of stable isotope reference samples. *Nature* **302**, 236–238.

Dauphas N. and Schauble E. A. (2016) Mass fractionation laws, mass-independent effects, and isotopic anomalies. *Annu. Rev. Earth Planet. Sci*. **44**, 709–83.

Ehrhardt H., Johannes W. and Seidel H. (1973) Hochdrucksynthese von Kupfer(II)-Carbonat. *Z. Naturforsch.* **28b**, 682.

Eiler J., Cartigny P., Hofmann A. E. and Piasecki A. (2013) Non-canonical mass laws in equilibrium isotopic fractionations: evidence from the vapor pressure isotope effect of SF_6. *Geochim. Cosmochim. Acta* **107**, 205–219.

Farquhar J., Thiemens M.H. and Jackson T. (1998) Atmosphere-surface interactions on Mars: $\Delta^{17}O$ measurements of carbonate from ALH 84001. *Science* **280**, 1580–1582.

Franchi I. A., Wright I. P., Sexton A. S. and Pillinger C. T. (1999) The oxygen-isotopic composition of Earth and Mars. *Meteorit. Planet. Sci*. **34**, 657–661.

Goldin D. M. and Kulikova G. V. (1984) On the dissociation mechanism of carbonates and their isomorphous mixture. *J. Thermal Anal*. **29** 139–145.

Haberkorn R., Michel-Beyerle M. E. and Michel K. W. (1977) Isotope effects in interstellar molecules by chemical hyperfine interaction. *Astron*. *Astrophys*. **55**, 315–318.

Hofmann M. E. G., Horváth B., Schneider L., Peters W., Schützenmeister K. and Pack A. (2017) Atmospheric measurements of $\Delta^{17}O$ in CO_2 in Göttingen, Germany reveal a seasonal cycle driven by biospheric uptake. *Geochim. Cosmochim. Acta* **199**, 143–163.

Hulston J. R. and Thode H. G. (1965) Variations in S^{33}, S^{34} and S^{36} contents of meteorites and their relation to chemical and nuclear effects. *J. Geophys. Res*. **70**, 3475–3484.

Kemper F., Jager C., Waters L., Henning T., Molster F. J., Barlow M. J., Lim T. and de Koter A. (2002) Detection of carbonates in dust shells around evolved stars. *Nature* **415**, 295–297.

Koplak O., Morgunov R. B. and Buchachenko A. L. (2013) Magnetic isotope and magnetic field effects on the silicon oxidation. *Chem. Phys. Lett*., **560**, 29−31.

Lander J. J. (1949) Polymorphism and anion rotational disorder in the alkaline earth carbonates. *J. Chem. Phys*. **17**, 892–901.

Lander J. J. (1951) The phase system BaO–$BaCO_3$. *J. Amer. Chem. Soc*. **73**, 5893–5894.

Lawler R. G. and Evans G. T. (1971) Chemical consequences of magnetic interactions in radical pairs. *Ind. Chim. Belge* **36**, 1087–1089.

Li Z., Zhao Z., Wang Q. and Wang G. (2018) Transition mechanism of the reaction interface of the thermal decomposition of calcite. *J. Cryst. Growth* **492**, 13–17.

Liu C, Liu T. and Wang D. (2018) Non-isothermal kinetics study on the thermal decomposition of brucite by thermogravimetry. *J. Thermal Anal. Calorim*. **134**, 2339–2347.

Matsuhisa Y., Goldsmith J. R. and Clayton R. N. (1978) Mechanisms of hydrothermal crystallization of quartz at 250°C and 15 kbar. *Geochim. Cosmochim. Acta* **42**, 173–182.

McCrea J. M. (1950) On the isotopic chemistry of carbonates and a paleotemperature scale. *J. Chem. Phys*. **18**, 849–857.

Meijer H. A. J. and Li W. J. (1998) The use of electrolysis for accurate $\delta^{17}O$ and $\delta^{18}O$ isotope measurements in water. *Isotopes Environ. Health Stud.* **34**, 349–369. Erratum: 1999 **35**, 142.

Miller M. F. (2002) Isotopic fractionation and the quantification of ^{17}O anomalies in the oxygen three-isotope system: an appraisal and geochemical significance. *Geochim. Cosmochim. Acta* **66**, 1881–1889.

Miller M. F. and Pack A. (2021) Why measure ^{17}O? Historical perspective, triple-isotope systematics and selected applications. In *Triple oxygen isotope geochemistry* (eds. I. N. Bindeman and A. Pack). *Rev. Mineral. Geochem.* **86**, Min. Soc. America. pp. 1–34.

Miller M. F., Buchachenko A. L., Bailey E., McMillan P. F. and Thiemens M. H. (2012) Investigating the possibility of a hyperfine coupling ('magnetic isotope effect') mechanism for the non-mass-dependent fractionation of oxygen isotopes caused by thermal decomposition of divalent metal carbonates. *Sixth Internatnl. Symp. Isotopomers (ISI 2012)*, Washington DC, USA. p.61 (abstr.). (https://www.yumpu.com/en/document/read/21466085/sixth-international-symposium-on-isotopomers-geophysical-)

Miller M. F., Franchi I. A., Sexton A. S. and Pillinger C. T. (1999) High precision $\delta^{17}O$ isotope measurements of oxygen from silicates and other oxides: method and applications. *Rapid. Commun. Mass Spectrom.* **13**, 1211–1217.

Miller M. F., Franchi I. A., Thiemens M. H., Jackson T. L., Brack A., Kurat G. and Pillinger C. T. (2002) Mass-independent fractionation of oxygen isotopes during thermal decomposition of carbonates. *Proc. Nat. Acad. Sci. U.S.A.* **99**, 10988–10993.

Miller M. F., Pack A., Bindeman I. N. and Greenwood R. C. (2020) Standardizing the reporting of $\Delta'^{17}O$ data from high precision oxygen triple-isotope ratio measurements of silicate rocks and minerals. *Chem. Geol*. 532, 119332.

Okumura T., Yoshimura M. and Kogure T. (2018) On the transition temperature to calcite and cell lengths for various biogenic aragonites. In: Endo, K., Kogure, T., Nagasawa, H. (editors) Biomineralization. Springer, Singapore, Chapter 1, pages 3–10. https://doi.org/10.1007/978-981-13-1002-7_1

Pack A., Tanaka R., Hering M., Sengupta S., Peters S. and Nakamura E. (2016) The oxygen isotope composition of San Carlos olivine on the VSMOW-SLAP2 scale. *Rapid Commun. Mass Spectrom*. **30**, 1495–1504.

Rao C. N. R., Prakash B. and Natarajan M. (1975) Crystal structure transformations in inorganic nitrites, nitrates and carbonates. *Nat. Stand. Ref. Data Series, Nat. Bur. Stand*. (U.S.A.) **53**, 48 pp.

Röckmann T., Brenninkmeijer C. A. M., Saueressig G., Bergamaschi P., Crowley J. N., Fischer H. and Crutzen P. J. (1998) Mass-independent oxygen isotope fractionation in atmospheric CO as a result of the reaction CO + OH. *Science* **281**, 544–546.

Rumble D., Miller M. F., Franchi I. A. and Greenwood R. C. (2007) Oxygen three-isotope fractionation lines in terrestrial silicate minerals: an inter-laboratory comparison of hydrothermal quartz and eclogitic garnet. *Geochim. Cosmochim. Acta* **71**, 3592–3600.

Salikhov K. M. (1996) *Magnetic isotope effect in radical reactions*: *an introduction*. Springer-Verlag, Wien.

Schoenemann S. W., Schauer A. J. and Steig E. J. (2013) Measurement of SLAP2 and GISP $\delta^{17}O$ and proposed VSMOW-SLAP normalization for $\delta^{17}O$ and $^{17}O_{excess}$. *Rapid Commun. Mass Spectrom.* **27**, 582–590.

Seidel von H., Viswanathan K., Johannes W. and Ehrhardt H. (1974) Darstellung, Struktur und Eigenschaften von Kupfer(II)-Carbonat. *Z. anorg. allg. Chem.* **410**, 138–148. (doi:10.1002/zaac.19744100207)

Shannon R. D. (1976) Revised effective ionic radii and systematic studies of interatomic distances in halides and chalcogenides. *Acta Crystallogr.* **A32**, 751–767.

Sharma T. and Clayton R. N. (1965) Measurement of O^{18}/O^{16} ratios of total oxygen of carbonates. *Geochim. Cosmochim. Acta* **29**, 1347–1353.

Sharp Z. D., Papike J. J. and Durakiewicz T. (2003) The effect of thermal decarbonation on stable isotope compositions of carbonates. *Amer. Mineral.* **88**, 87–92.

Speer J. A. (1983) Crystal chemistry and phase relations of orthorhombic carbonates. In *Carbonates: Mineralogy and Chemistry* (ed. R. J. Reeder). *Rev. Mineral. Geochem.* **11**, Min. Soc. America. pp. 145–189.

Suits A. G. (2020) Roaming reactions and dynamics in the van der Waals region. *Annu. Rev. Phys. Chem.* **71**, 77–100.

Sun T. and Bao H. (2011a) Non-mass-dependent ^{17}O anomalies generated by a superimposed thermal gradient on rarefied O_2 in a closed system. *Rapid Commun. Mass Spectrom.* **25**, 20–24.

Sun T. and Bao H. (2011b) Thermal-gradient-induced non-mass-dependent isotope fractionation. *Rapid Commun. Mass Spectrom.* **25**, 765–773.

Tanaka R. and Nakamura E. (2013) Determination of ^{17}O-excess of terrestrial silicate/oxide minerals with respect to Vienna Standard Mean Ocean Water (VSMOW). *Rapid Commun. Mass Spectrom.* **27**, 285–297.

Thiemens M. H. and Heidenreich J. E. III. (1983) The mass-independent fractionation of oxygen: a novel isotope effect and its possible cosmochemical implications. *Science* **219**, 1073–1075.

Thiemens M. H. and Lin M. (2019) Use of isotope effects to understand the present and past of the atmosphere and climate and track the origin of life. *Angew. Chem.* (*Int. Ed*.) **58**, 6826–6844.

Timmel C. R. and Henbest K. B. (2004) A study of spin chemistry in weak magnetic fields. *Phil Trans. Roy. Soc. Lond. A* **362**, 2573–2589.

Toppani A., Robert F., Libourel G., de Donato P., Barres O., d'Hendecourt L. and Ghanbaja J. (2005) A 'dry' condensation origin for circumstellar carbonates. *Nature* **437**, 1121–1124.

Townsend D., Lahankar S. A., Lee S. K., Chambreau S. D., Suits A. G., Zhang X., Rheinecker J., Harding L. B. and Bowman J. M. (2004) The roaming atom: straying from the reaction path in formaldehyde decomposition. *Science* **306**, 1158–1161.

Turro N. J., Cheng C-C., Wan P., Chung C. and Mahler W. (1985) Magnetic isotope effects in the photolysis of dibenzyl ketone on porous silica. ^{13}C and ^{17}O enrichments. *J. Phys. Chem*. **89**, 1567–1568.

Urey H. C. (1947) The thermodynamic properties of isotopic substances. *J. Chem. Soc*. 562–581.

Wang D., Zhao Z., Tan G. L., Zhang S. and Wang Q. (2017) An investigation of the decomposition mechanism of calcium carbonate. *Metalurgija* **56**, 9–12.

Wen J. and Thiemens M. H. (1991) Experimental and theoretical study of isotope effects on ozone decomposition. *J. Geophys. Res*. **96** (D6), 10911–10921.

Woodward J. R. (2002) Radical pairs in solution. *Prog. React. Kinet. Mech*. **27**, 165–207.

Yeung L. Y. and Hayles J. A. (2021) Climbing to the top of Mount Fuji: uniting theory and observations of oxygen triple isotope systematics. In *Triple oxygen isotope geochemistry* (eds. I. N. Bindeman and A. Pack). *Rev. Mineral. Geochem.* **86**, Min. Soc. America. pp. 97–135.

Yoshioka S. and Kitano Y. (1985) Transformation of aragonite to calcite through heating. *Geochem. J*., **19**, 245–249.

Young E. D., Galy A. and Nagahara H. (2002) Kinetic and equilibrium mass-dependent isotope fractionation laws in nature and their geochemical and cosmochemical significance. *Geochim. Cosmochim. Acta* **66**, 1095–1104.

Zel'dovich Va. B. and Maksimov I. A. (1976) Gas diffusion: its dependence on nuclear spin. *Soviet J. Experiment. Theoret. Phys*. **43**, 39–41.

Zhao Z., Li Z., Wang Q. and Wang Y. (2015) Quantum chemical study of thermal decomposition mechanism and polymorph predict phase transitions of magnesite. *Res Chem. Intermed*. **41**, 8471–8482.

Zhao Z., Wang D., Wang Q., Li Z. and Fang Z. (2013) Quantum chemical study on thermal decomposition mechanism of calcium carbonate. *J. Theoret. Computat. Chem*. **12** (6), 1350049. (doi: 10.1142/S0219633613500491)

Zsakó J. (1968) Kinetic analysis of thermogravimetric data. *J. Phys. Chem*. **72** (7), 2406–2411.

Table 1

Sample details. Apart from the magnesite and dolomite samples, which were used in the previous investigation (Miller et al., 2002), all natural carbonate mineral specimens were provided from the Mineralogy collection of the Natural History Museum, London.

Sample		Museum reference	Origin
Rhombohedral carbonates			
Magnesite	$MgCO_3$	SC654 (NHM Wien)	Hydrothermal origin, Oberdorf an der Laming, Styria, Austria
Calcite	$CaCO_3$	BM.1973,514	Cyrus mine, Yavapai County, Arizona, U.S.A.
Rhodochrosite	$MnCO_3$	BM.1907,640	Lake County, Colorado, U.S.A.
Siderite	$FeCO_3$	BM.1905,147	Allevard, Isère, France
Smithsonite	$ZnCO_3$	BM.1929,1754	Kabwe ('Broken Hill') mine, Kabwe, Central Province, Zambia
Dolomite	$Ca,Mg(CO_3)_2$	Not applicable	Fine-grained sample from base of Mt. Lagazuoi, Belluno, Italy
Orthorhombic carbonates			
Aragonite	$CaCO_3$	BM.83863	Sterkfontein caves, Barnett, Transvaal, South Africa
Strontianite	$SrCO_3$	BM.1907,638	Drensteinfurt, Munster, North Rhine-Westphalia, Germany
Cerussite	$PbCO_3$	BM.1968,662	Tsumeb, Oshikoto, Namibia
Witherite	$BaCO_3$	BM.69131	Fallowfield mine, Hexham, Northumberland, U.K.

Table 2

Oxygen triple-isotope compositions of the solid oxides formed from carbonate thermal decomposition, together with the corresponding data from CO_2 released during $CuCO_3$ thermolysis.

Carbonate	Solid oxide	$\delta^{17}O$ (‰)	SE	$\delta^{18}O$ (‰)	SE	$\delta^{18}O$ shift (‰)	$\Delta'^{17}O$ (‰)
Rhombohedral structure							
Magnesite	MgO	*9.203*	*0.013*	*18.203*	*0.007*	*–2.1*	*–0.292*
		9.716	*0.018*	*19.197*	*0.004*	*–1.1*	*–0.295*
		10.476	0.009	20.635	0.006	0.4	–0.281
		11.320	0.024	22.289	0.012	2.0	–0.295
Calcite	CaO	9.743	0.005	19.175	0.003	3.0	–0.257
		9.163	0.009	18.070	0.007	1.9	–0.263
		8.511	0.013	16.927	0.003	0.8	–0.321
Rhodochrosite	MnO	4.035	0.022	8.355	0.007	–1.8	–0.333
		3.798	0.007	7.934	0.007	–2.2	–0.350
Siderite	FeO	8.652	0.011	17.341	0.004	2.8	–0.394
		8.458	0.005	16.989	0.007	2.5	–0.405
	§ *	7.983	0.011	15.857	0.002	1.3	–0.293
	§ *	8.218	0.009	16.322	0.013	1.8	–0.299
	*	8.425	0.006	16.694	0.003	2.2	–0.286
	*	8.361	0.016	16.593	0.003	2.1	–0.297
Smithsonite	ZnO	15.283	0.004	30.001	0.006	4.6	–0.322
		15.393	0.012	30.236	0.005	4.8	–0.333
Dolomite	(Ca,Mg)O	*16.571*	*0.014*	*32.583*	*0.007*	*2.3*	*–0.366*
		17.017	*0.022*	*33.441*	*0.009*	*3.2*	*–0.363*
		17.124	*0.009*	*33.575*	*0.004*	*3.3*	*–0.325*
		17.182	*0.015*	*33.745*	*0.014*	*3.5*	*–0.354*
		16.426	0.008	32.163	0.011	1.9	–0.296
		16.556	0.024	32.425	0.009	2.2	–0.301
Orthorhombic structure							
Aragonite	CaO	11.349	0.014	22.515	0.008	–3.3	–0.382
		13.550	0.010	26.708	0.006	0.9	–0.352
Strontianite	SrO	15.540	0.016	30.586	0.005	6.0	–0.366
		15.565	0.019	30.577	0.005	6.0	–0.337
		14.022	0.013	27.676	0.004	3.1	–0.381
		14.989	0.011	29.640	0.005	5.1	–0.428
Cerussite	PbO	1.869	0.026	4.333	0.006	–7.5	–0.398
		1.969	0.008	4.513	0.006	–7.3	–0.392
	§ *	1.799	0.015	4.112	0.005	–7.7	–0.353
	§ *	1.721	0.012	3.904	0.005	–7.9	-0.322
Witherite	BaO	3.541	0.007	7.458	0.014	–9.1	–0.359
		–0.048	0.013	0.580	0.007	–16.0	–0.352
Monoclinic structure							
Copper carbonate	CuO (#1)	7.443	0.017	14.702	0.007	–	–0.232
	(#2)	7.604	0.018	14.945	0.007	(–2.45)	–0.198
	(#3)	7.708	0.015	15.202	0.008	(–2.32)	–0.227
	CO_2 released by thermal decomposition of the $CuCO_3$:						
	(#2)	9.798	–	18.619	–	(1.23)	0.084
	(#3)	9.856	–	18.676	–	(1.16)	0.112
	Isotopic composition of the $CuCO_3$, inferred from the CuO and CO_2 data:						
	(#2)	9.067	–	17.394	–	–	–0.010
	(#3)	9.140	–	17.518	–	–	–0.001

Notes: Data in italics are reproduced from Miller et al. (2002). 'SE' refers to standard error.
Data in parentheses are derived from the inferred $\delta^{17}O$ and $\delta^{18}O$ values of the synthesised $CuCO_3$.
§ Pyrolysis conducted in the presence of an applied static magnetic field of flux density ~250 mT.
* Pyrolysis conducted using a different extraction line, tube furnace design and heating duration (see text).

Fig. 1

Mass-dependent relationship between the oxygen triple-isotope compositions of the metal oxides formed from thermal decomposition of the various natural carbonate samples. Data points represent the mean of replicates; individual measurements are reported in Table 2. Error bars indicate the respective ranges obtained from replicates. For PbO, MnO and ZnO, the error bars are of similar size, or smaller than, the associated data point symbols. Tight coupling of the respective ordinate and abscissa data – as a result of the fractionation conforming to 'mass-dependent' norms – resulted in deviations from the least squares linear regression line being of very small magnitude: all ordinate deviations were within the range –0.044 to +0.057. Uncertainties of the slope and intercept values of the regression line are reported as standard error.

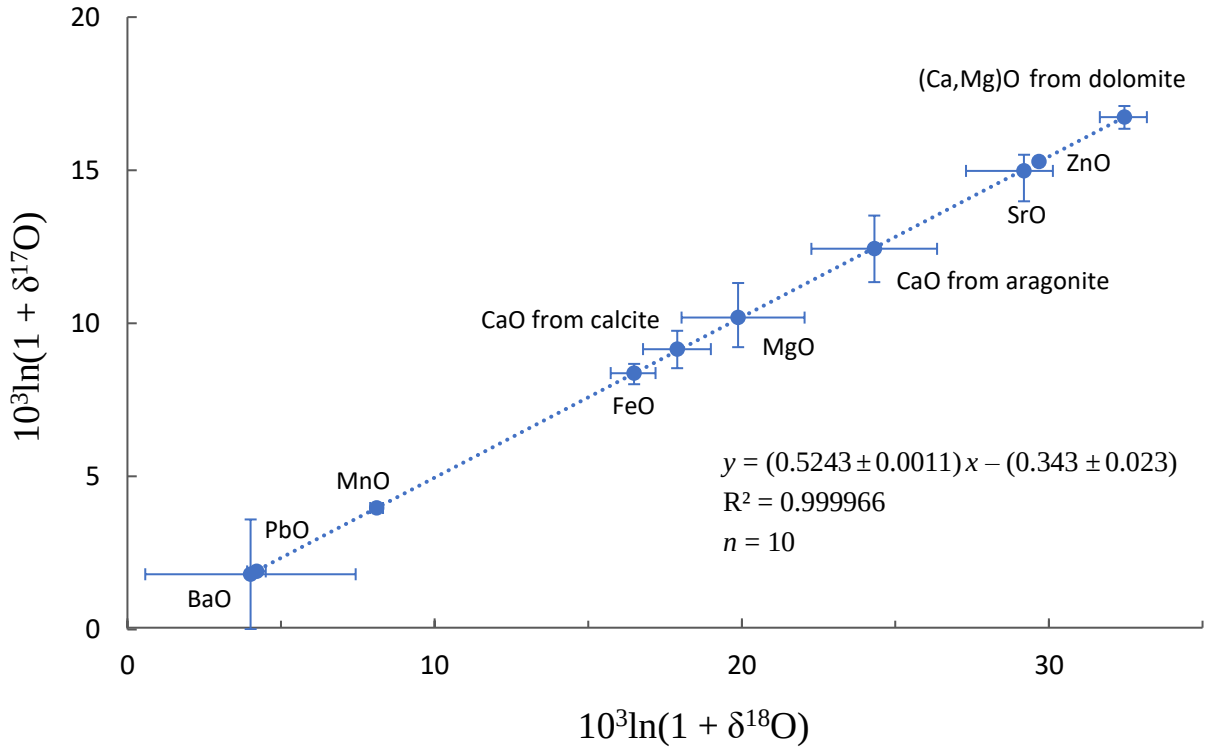

Fig. 2

Relationship between the oxygen triple-isotope compositions of CuO and CO_2 formed from thermal decomposition of replicate grains of the synthesised $CuCO_3$ sample, together with the inferred oxygen isotopic composition of the $CuCO_3$.

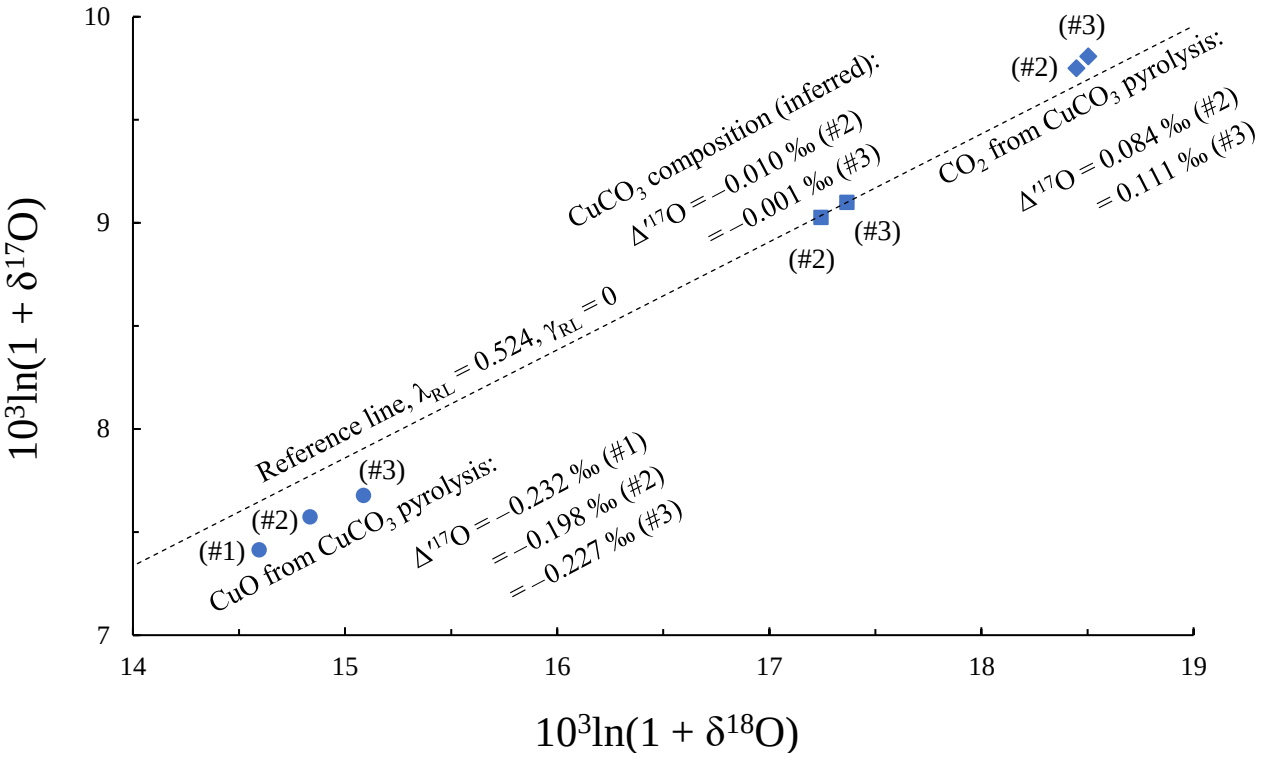

Fig. 3

CO_2 thermal evolution profiles of the natural carbonate specimens (crushed to a fine grain size) as a function of heating temperature (ramp rate 0.5 °C min^{-1}) in helium flow (53.8 mL min^{-1}). Individual peak temperatures are labelled in parentheses, together with the carbonate mass (mg) used. Uniquely, a bimodal release of CO_2 was observed from witherite; the initial (broad) peak maximum was at ~950 °C.

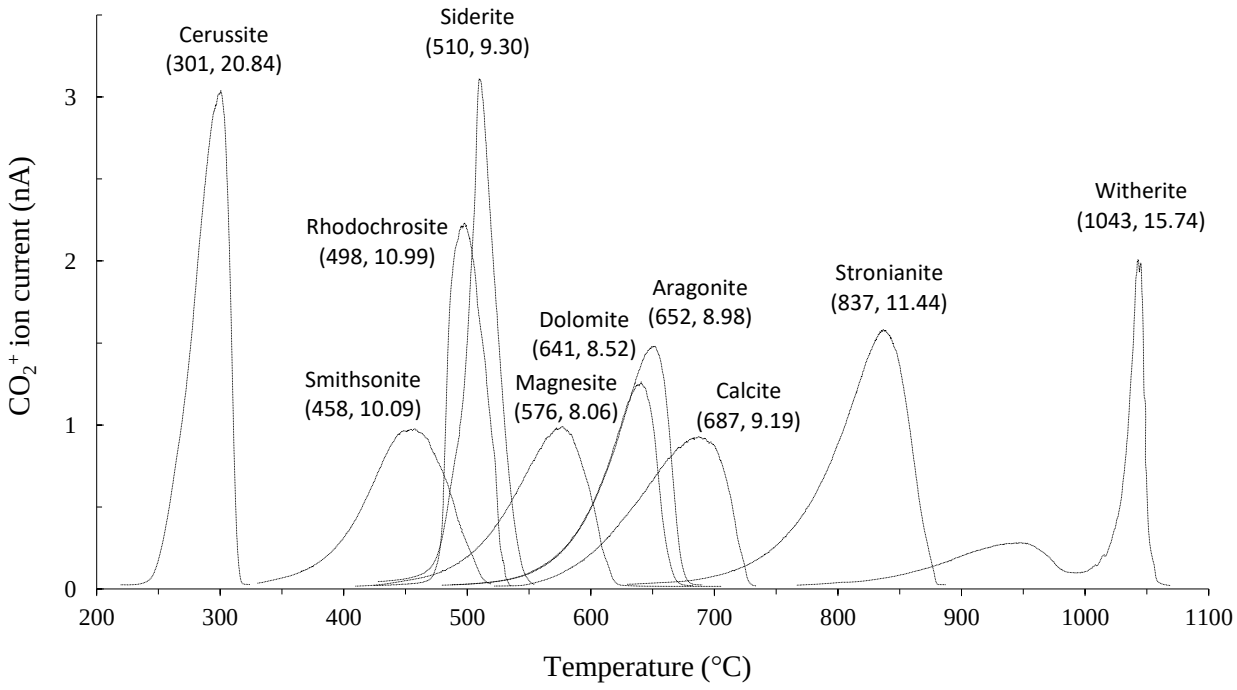

Fig. 4

Illustrating the relative thermal stabilities of the natural carbonate examples used in this investigation, as exemplified by the temperature at which maximum CO_2 evolution occurred during TGA/EGA, with heating at a ramp rate of 0.5 °C min^{-1} in a flow of helium. Also shown are the individual replicate data points, indicating the respective shifts in $\delta^{18}O$ accompanying the carbonate to solid oxide transformation.

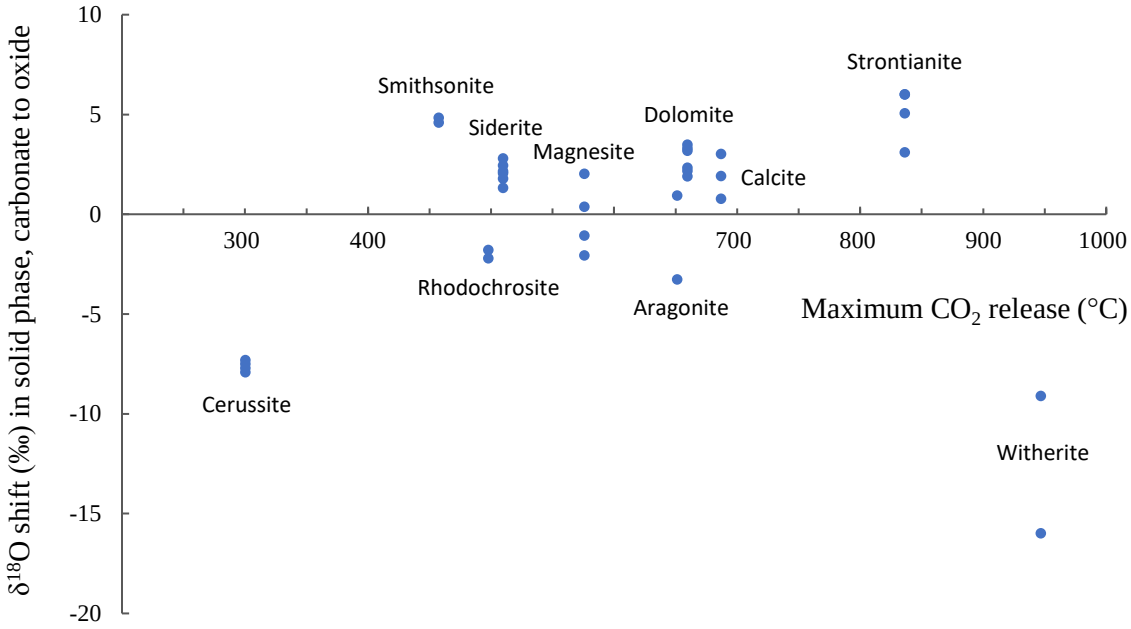

Fig. 5

Illustrating the relationship between carbonate structural group (as determined by the cation radius) and the $\Delta'^{17}O$ value of the metal oxide produced by thermal decomposition of the corresponding carbonate mineral. Solid oxide $\Delta'^{17}O$ data produced from rhombohedral carbonates are denoted by ●, whereas orthorhombic examples are shown as ■. The sole example characterised by a monoclinic structure for the carbonate is illustrated by ◆. Cation radius data are from Shannon (1976). The mean $\Delta'^{17}O$ value of the metal oxides derived from thermal decomposition of the rhombohedral carbonates (calcite and isotypes) and orthorhombic carbonates (aragonite and isotypes) are denoted by -------- and -------- respectively. Similarly, -------- shows the mean $\Delta'^{17}O$ value of the CuO replicates produced from thermal decomposition of $CuCO_3$.

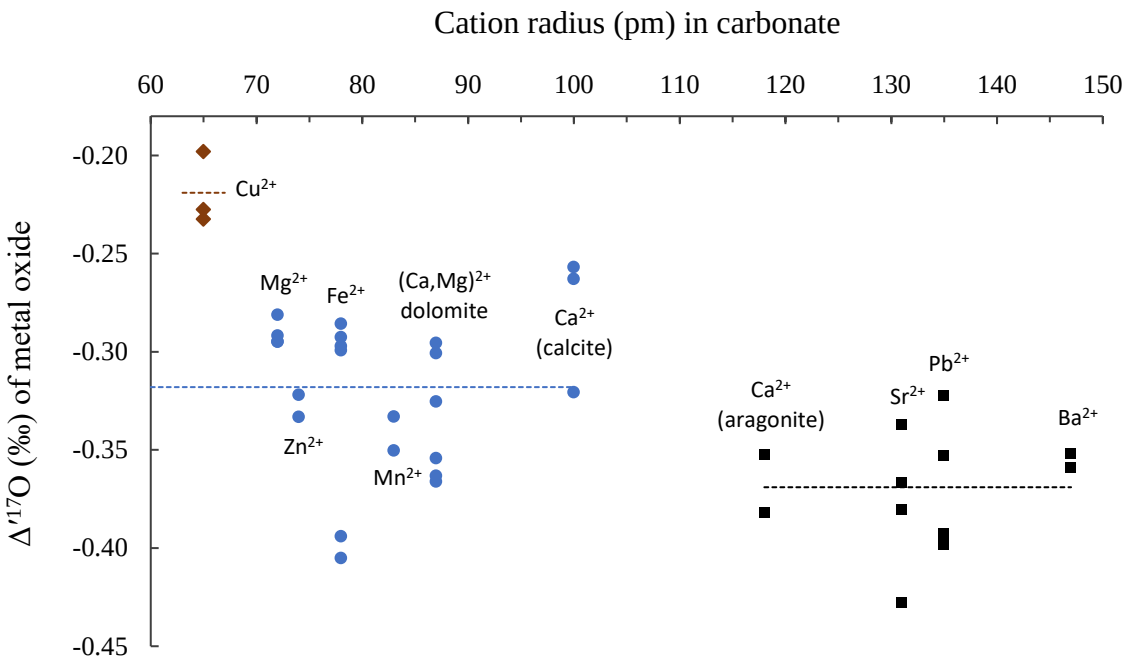

Fig. 6

Illustrating the lack of a systematic relationship between the $\Delta'^{17}O$ values of the divalent metal oxides produced by carbonate thermal decomposition and the corresponding linearised $\delta^{18}O$ values. Also shown are the data from CO_2 released during thermal decomposition of $CuCO_3$, together with recently-reported results (Miller et al., 2020) from silicate standards San Carlos olivine and UWG-2 garnet, for comparison. Symbols are as defined for Fig. 5.

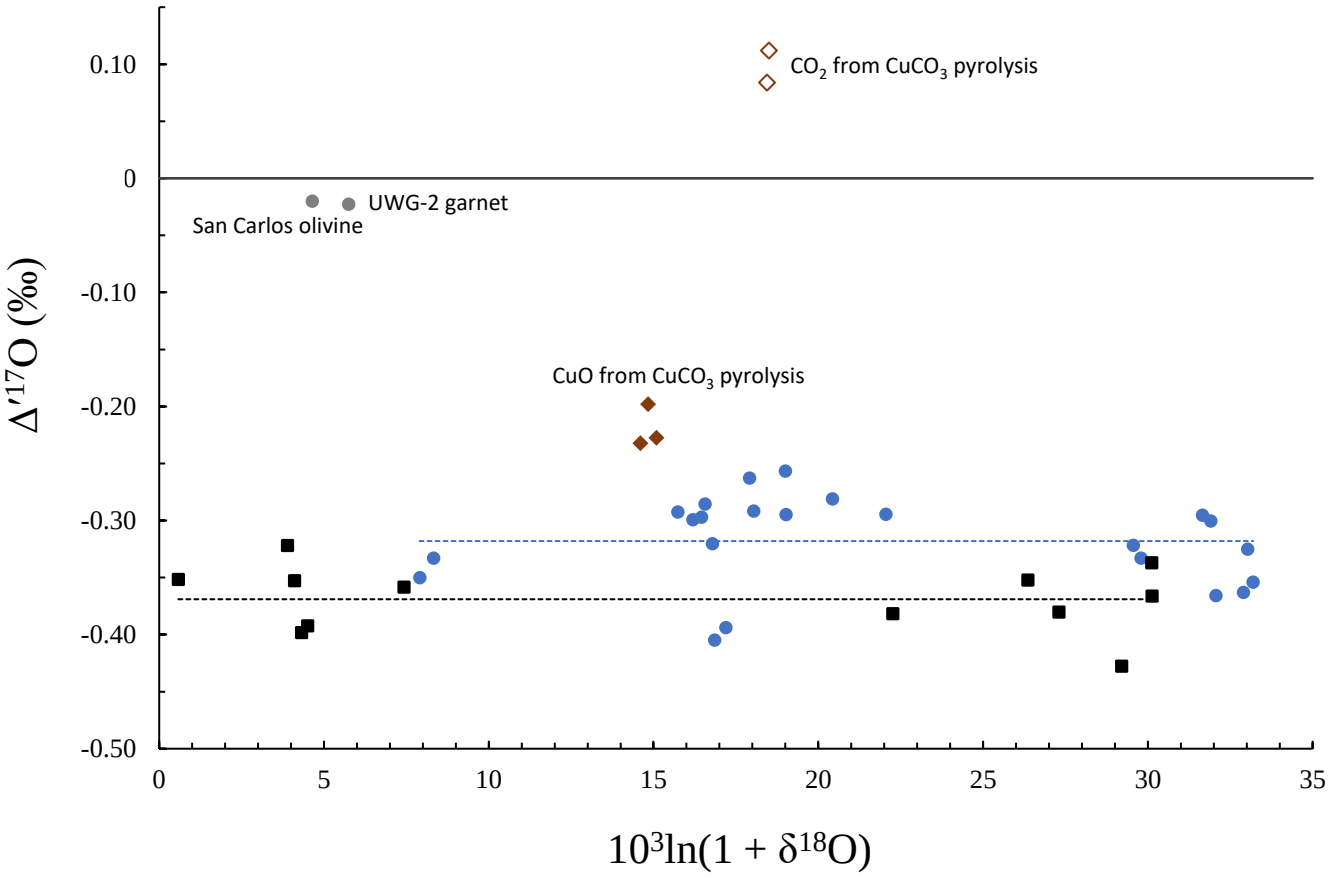

Fig. 7

Proposed simple model reaction mechanism for the thermal decomposition of metal carbonates. k_{vac} is the first order rate coefficient for the arrival of vacancies at the site of a vibrationally excited carbonate ion (incorporating the concentration of vacancies). Vacancies are lost as they diffuse away from the carbonate, with rate coefficient k_{-vac}. The forward and back rate coefficients for the movement of the carbonate ion radical between the vacancy and original sites are designated as k_{jump} and k_{-jump} respectively; these coefficients are set to be equal, i.e. assuming equal probability for 'jumping' between the sites in either direction. k_f is the rate coefficient for the forward electron transfer reaction (which is spin-state selective and takes place only from the singlet ion radical pair). k_{ST} is a simple, first order rate coefficient which approximates the coherent spin-state mixing process of singlet and triplet radical pairs. k_{rlx} is the rate of the return of triplet state close pairs to the carbonate ion due to incoherent electron spin relaxation. It is included for completeness and can influence the size of the observed isotope effect.

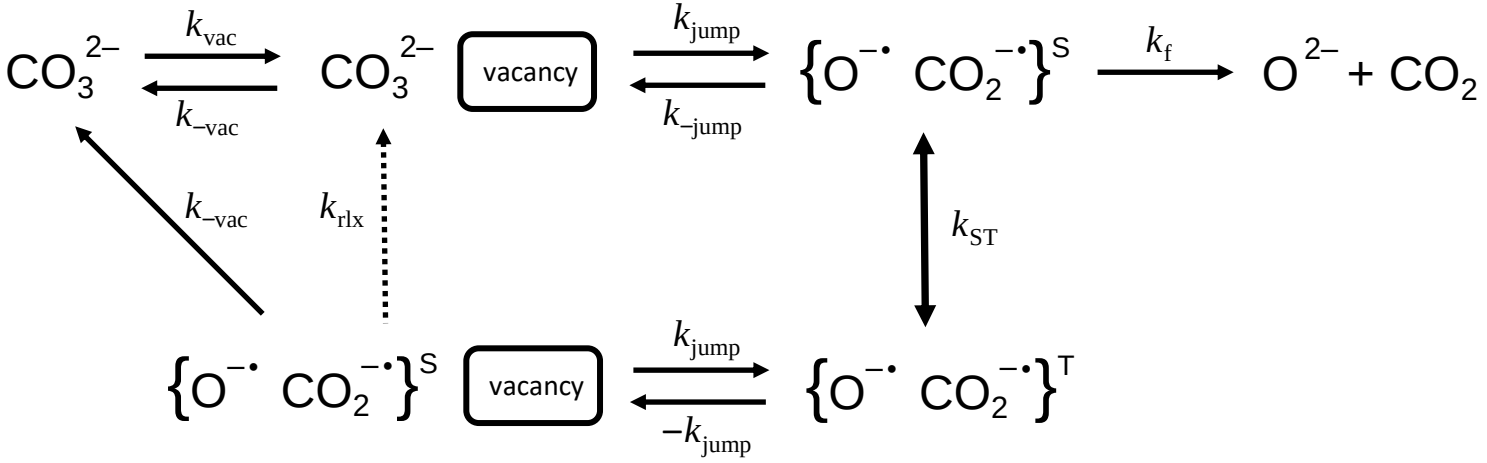

Fig. 8

Explicit representation of the scheme presented in Fig. 7 for the case of a carbonate ion containing ^{17}O. The most abundant isotope of oxygen, ^{16}O, is shown without the associated mass number. Two radical pairs are possible, produced in a 1:2 ratio. These undergo spin-state mixing at different rates (k_{ST1} and k_{ST2}), resulting in a difference in the respective yields of the two products.

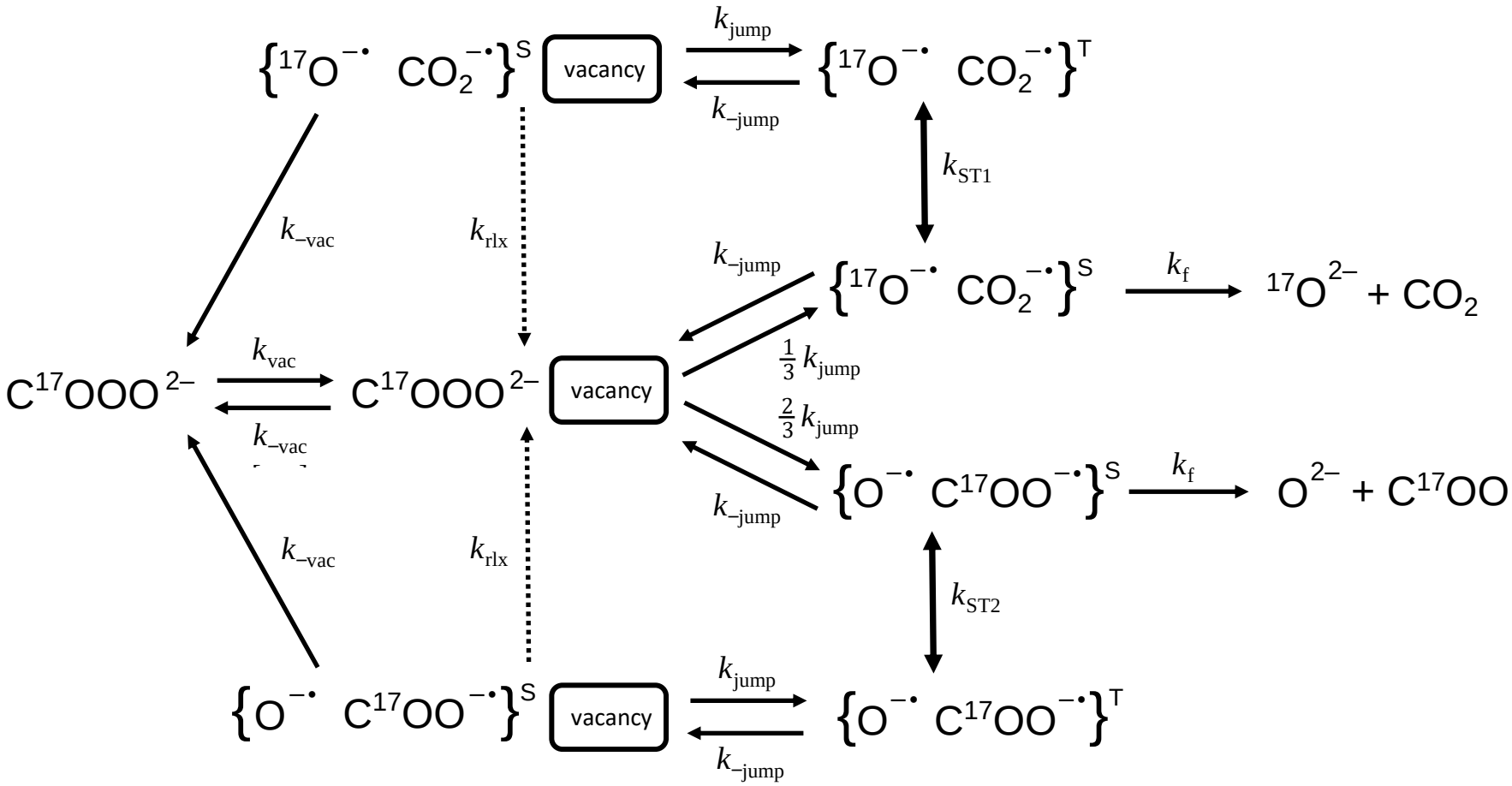

Fig. 9

Numerical simulation of the kinetic scheme presented in Fig. 8. Parameters were selected to be physically reasonable and produce a substantial magnetic isotope effect for clarity (adjusting the parameters over a reasonable range can control the size of the effect). The following values were used: $k_{jump} = 10^9\ s^{-1}$, $k_f = 10^8\ s^{-1}$, $k_{ST1} = 1.5 \times 10^9\ s^{-1}$, $k_{ST2} = 1.0 \times 10^9\ s^{-1}$, $k_{rlx} = 1.0 \times 10^6\ s^{-1}$. The values of k_{vac} and $-k_{vac}$ affect the long timescale behaviour over which the decomposition occurs, but do not change the magnitude of the isotope effect. k_{vac} was set to be $10^{-3}\ s^{-1}$, to give an overall decomposition timescale of similar magnitude to the experimental data. $-k_{vac}$ was arbitrarily set to $10^2\ s^{-1}$, as it has a negligible effect on the shape of the curves when large relative to k_{vac}, but slow relative to all the other processes.

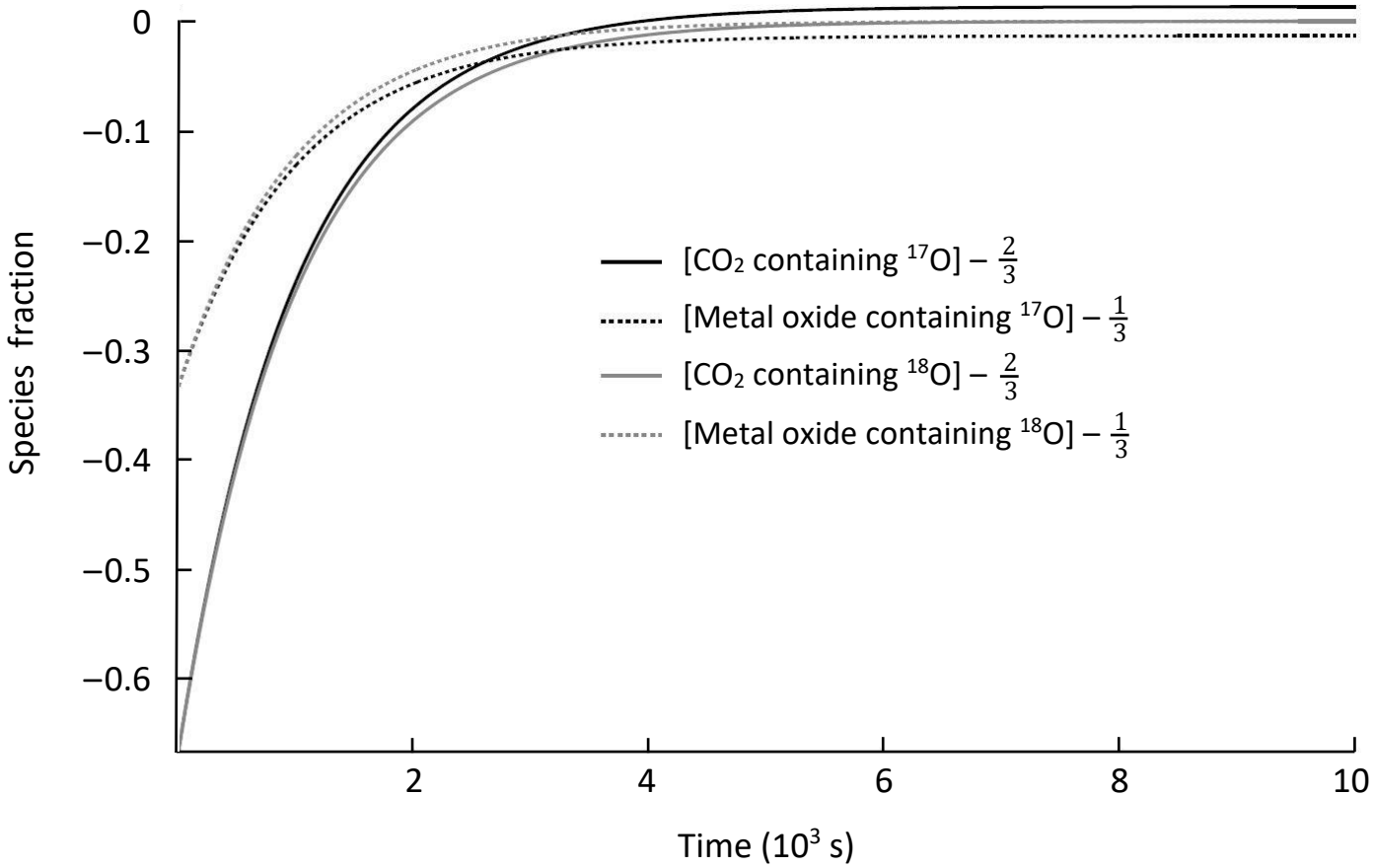

APPENDIX A.

Table A.1 Results of $\delta^{18}O$ measurements of the natural carbonate specimens.

Carbonates were reacted with concentrated H_3PO_4 under temperature-controlled conditions (McCrea, 1950) and the evolved CO_2 analysed for $\delta^{13}C$ and $\delta^{18}O$. The various fractionation factors (α) used to determine the $\delta^{18}O$ values of the carbonates from the isotopic measurements of CO_2 are listed, together with the corresponding literature reference. Samples were in the form of either small grains (sg) or powders (p). The $\delta^{18}O$ value of the dolomite has been reported previously (Miller et al., 2002) as 30.26 ‰ relative to VSMOW.

Sample	mass (mg)		Reaction T (°C)	CO_2 $\delta^{18}O_{VPDB}$ (‰)	α	Ref.	Carbonate $\delta^{18}O_{VPDB}$ (‰)	Carbonate $\delta^{18}O_{VSMOW}$ (‰)	Carbonate $\delta^{18}O_{VSMOW}$ mean (‰)
Calcite	1.4994	sg	25.0	–4.031	1.0105	[a]	–14.380	16.086	
	1.4160	sg	25.0	–3.986			–14.335	16.131	16.15
	2.7521	p	25.2	–3.884			–14.235	16.235	
Aragonite	1.3780	sg	25.0	6.145	1.01107	[a]	–4.871	25.888	
	1.5100	sg	25.2	6.039			–4.976	25.780	
	1.4748	sg	25.2	6.000			–5.014	25.741	25.78
	2.8385	p	25.2	5.984			–5.030	25.724	
Cerussite	3.6429	p	50	–8.966	1.00976	[b]	–18.545	11.792	
	3.3191	p	50	–8.882			–18.462	11.878	11.83
	3.4920	p	50	–8.940			–18.519	11.818	
Siderite	2.7600	p	150	–8.248	1.00771	[c]	–15.836	14.585	
	2.7980	p	150	–8.309			–15.896	14.522	14.54
	2.4406	p	150	–8.307			–15.894	14.524	
Rhodochrosite	3.1757	p	60	–12.450	1.008554	[d]	–20.006	10.286	
	3.0694	p	60	–12.567			–20.122	10.166	10.14
	3.1140	p	60	–12.775			–20.328	9.953	
Strontianite	3.7424	p	60	2.800	1.008894	[d]	–6.040	24.683	
	3.8474	p	60	2.441			–6.396	24.316	24.58
	3.8700	p	60	2.851			–5.990	24.735	
Smithsonite	2.9504	p	50	5.006	1.01042	[b]	–5.358	25.386	
	2.7265	p	50	5.050			–5.315	25.431	25.41
Witherite	4.7640	p	60	5.006	1.009935	[d]	–4.881	25.879	
	4.8831	p	60	5.050			–4.837	25.924	22.80
	5.0300	p	60	–4.078			–13.875	16.606	
Magnesite	3.9579	p	100	–1.237	1.009228	[e]	–10.369	20.220	
	4.2163	p	100	–1.036			–10.170	20.425	
	3.9391	p	100	–1.289			–10.421	20.167	20.26
	4.0440	p	100	–1.230			–10.362	20.227	

Sources of fractionation factors: [a]. Kim S-T. and O'Neil J. R. (1997) Equilibrium and nonequilibrium oxygen isotope effects in synthetic carbonates. *Geochim. Cosmochim. Acta* **61**, 3461–3475; [b]. Gilg H. A., Struck U., Vennemann T. and Boni M. (2003) Phosphoric acid fractionation factors for smithsonite and cerussite between 25 and 72 °C. *Geochim. Cosmochim. Acta* **67**, 4049–4055; [c]. Rosenbaum J. and Sheppard S. M. F. (1986) An isotopic study of siderites, dolomites and ankerites at high temperatures. *Geochim. Cosmochim. Acta* **50**, 1147–1150; [d]. Böttcher M. (1996) $^{18}O/^{16}O$ and $^{13}C/^{12}C$ fractionation during the reaction of carbonates with phosphoric acid: effects of cationic substitution and reaction temperature. *Isot. Environ. Health Stud*. **32**, 299–305; [e]. Das Sharma S., Patil D. J. and Gopalan K. (2002) Temperature dependence of oxygen isotope fractionation of CO_2 from magnesite-phosphoric acid reaction. *Geochim. Cosmochim. Acta* **66**, 589–593.

Table A.2 Stable isotopes of cation elements in the carbonate specimens.

Isotope	Atomic mass (Da)	Natural abundance (atom %)	Nuclear spin (I)	Magnetic moment (μ/μN)	Electronic structure (gas, ground state)
^{24}Mg	23.9850423	78.99	0	0	
^{25}Mg	24.9858374	10.00	5/2	–0.85546	[Ne] $3s^2$
^{26}Mg	25.9825937	11.01	0	0	
^{40}Ca	39.9625906	96.941	0	0	
^{42}Ca	41.9586176	0.647	0	0	
^{43}Ca	42.9587662	0.135	7/2	–1.31727	[Ar] $4s^2$
^{44}Ca	43.9554806	2.086	0	0	
^{46}Ca	45.953689	0.004	0	0	
^{48}Ca	47.952533	0.187	0	0	
^{55}Mn	54.9380471	100	5/2	3.4532	[Ar] $3d^5\,4s^2$
^{54}Fe	53.9396127	5.845	0		
^{56}Fe	55.9349393	91.754	0		
^{57}Fe	56.9353958	2.119	1/2	0.09062294	[Ar] $3d^6\,4s^2$
^{58}Fe	57.9332773	0.282	0		
^{63}Cu	62.9295989	69.17	3/2	2.2233	[Ar] $3d^{10}\,4s^1$
^{65}Cu	64.9277929	30.83	3/2	2.3817	
^{64}Zn	63.9291448	48.63	0		
^{66}Zn	65.9260347	27.90	0		
^{67}Zn	66.9271291	4.10	5/2	0.875479	[Ar] $3d^{10}\,4s^2$
^{68}Zn	67.9248459	18.75	0		
^{70}Zn	69.925325	0.62	0		
^{84}Sr	83.913430	0.56	0		
^{86}Sr	85.9092672	9.86	0		
^{87}Sr	86.9088841	7.00	9/2	–1.09283	[Kr] $5s^2$
^{88}Sr	87.9056188	82.58	0		
^{130}Ba	129.906282	0.106	0		
^{132}Ba	131.905042	0.101	0		
^{134}Ba	133.904486	2.417	0		
^{135}Ba	134.905665	6.592	3/2	0.837943	[Xe] $6s^2$
^{136}Ba	135.904553	7.854	0		
^{137}Ba	136.905812	11.232	3/2	0.937365	
^{138}Ba	137.905232	71.698	0		
^{204}Pb	203.973020	1.4	0		
^{206}Pb	205.974440	24.1	0		
^{207}Pb	206.975872	22.1	1/2	0.58219	[Xe] $4f^{14}\,5d^{10}\,6s^2\,6p^2$
^{208}Pb	207.976627	52.4	0		

Data source: www.webelements.com